Western Kentucky University
TopSCHOLAR®

Masters Theses & Specialist Projects | Graduate School

8-2012

Application of the Weather Research and Forecasting (WRF) Model to Simulate a Squall Line: Implications of Choosing Parameterization Scheme Combinations and Model Initialization Data Sets

Mitchell Gaines
Western Kentucky University, mitchell.gaines673@topper.wku.edu

Follow this and additional works at: http://digitalcommons.wku.edu/theses

 Part of the Meteorology Commons

Recommended Citation
Gaines, Mitchell, "Application of the Weather Research and Forecasting (WRF) Model to Simulate a Squall Line: Implications of Choosing Parameterization Scheme Combinations and Model Initialization Data Sets" (2012). *Masters Theses & Specialist Projects.* Paper 1181.
http://digitalcommons.wku.edu/theses/1181

This Thesis is brought to you for free and open access by TopSCHOLAR®. It has been accepted for inclusion in Masters Theses & Specialist Projects by an authorized administrator of TopSCHOLAR®. For more information, please contact topscholar@wku.edu.

APPLICATION OF THE WEATHER RESEARCH AND FORECASTING (WRF) MODEL TO SIMULATE A SQUALL LINE: IMPLICATIONS OF CHOOSING PARAMETERIZATION SCHEME COMBINATIONS AND MODEL INITIALIZATION DATA SETS

A Thesis
Presented to
The Faculty of the Department of Geography and Geology
Western Kentucky University
Bowling Green, Kentucky

In Partial Fulfillment
Of the Requirements for the Degree
Master of Science

By
Mitchell Gaines

August 2012

APPLICATION OF THE WEATHER RESEARCH AND FORECASTING (WRF) MODEL TO SIMULATE A SQUALL LINE: IMPLICATIONS OF CHOOSING PARAMETERIZATION SCHEME COMBINATIONS AND MODEL INTIALIZATION DATA SETS

Date Recommended 04/23/12

Dr. Rezaul Mahmood, Director of Thesis

Dr. Josh Durkee

Dr. Xingang Fan

Dr. Stuart Foster

7-10-12

Dean, Graduate Studies and Research Date

ACKNOWLEDGMENTS

I would like to take this opportunity to thank Dr. Arturo Quintanar and Mr. William Rodgers, researchers with the Kentucky Climate Center research lab at Western Kentucky University, for their assistance with graphics development. My sincere thanks goes to T.J. Malone, meteorologist at Meridan Environmental Technology, Inc., Grand Forks, ND and WKU graduate, for providing valuable research notes from a study similar to that presented in Chapter Three. I would also like to thank my colleagues at the National Weather Service in Mt. Holly, NJ for their assistance in developing a PowerPoint presentation for an early draft of this thesis. Special thanks also goes out to Mr. Ronnie Leeper with the National Oceanic and Atmospheric Administration.

I am particularly grateful to my thesis committee members, all of whom have spent valuable time over the past several semesters as counsel for this project. I am especially indebted to Dr. Rezaul Mahmood, my thesis advisor, for his invaluable assistance and guidance throughout the process of graduate school and the preparation of this work for publication. Thanks also go out to Dr. David Keeling, head of WKU's Geography and Geology department and Bruce Kessler of WKU's Odgen College of Science and Engineering for securing funding for several conference trips throughout the process of this research. It is important that I also acknowledge Wendy De Croix for her assistance with various administrative matters. I would like to acknowledge Sami Almundaris, Ian Blaylock, Josh Gilliand, Andrew McKaughan, Kyle Thompson and Jeremy Young for their input on various issues on this thesis. On a personal level I would like to acknowledge the college readers Jennifer Anderson and Patricia Reynolds along with my parents, Woody and Lois Gaines, for their support.

TABLE OF CONTENTS

LIST OF FIGURES

LIST OF TABLES

APPLICATION OF THE WEATHER RESEARCH AND FORECASTING (WRF) MODEL TO SIMULATE A SQUALL LINE: IMPLICATIONS OF CHOOSING PARAMETERIZATION SCHEME COMBINATIONS AND MODEL INTIALIZATION DATA SETS

Mitchell Gaines August 2012 72 Pages

Directed by: Drs. Rezaul Mahmood, Josh Durkee, Xingang Fan, Stuart Foster

Department of Geography and Geology Western Kentucky University

On January 29-30, 2008 a squall line of thunderstorms moved through the Ohio Valley resulting in four deaths and one injury. Such events highlight the importance of accurate forecasting for public safety. Mesoscale Modeling plays an important role in any forecast of a potential squall line. The focus of this study was to examine the performance of several parameterization scheme combinations in the Weather Research and Forecasting Model version three (WRF) as they related to this event. These examinations included cloud microphysics (WRF Single-Moment 3-class, 6-class, and Goddard), cumulus parameterization (Kain-Fritsch and Bets-Miller-Janjic) and planetary boundary layer schemes (Yonsei-University and Mellor-Yamada-Janjic). A total of 12 WRF simulations were conducted for all potential scheme combinations. Data from the WRF simulations for several locations in south central Kentucky were analyzed and compared using Kentucky Mesonet observations for four locations: Bowling Green, Russellville, Murray and Liberty, KY. A fine model resolution of 1 km was used over these locations. Coarser resolutions of 3 km and 9 km were used on the outer two domains, which encompassed the Ohio and Tennessee Valleys. The model simulation performance was assessed using established statistical measures for the above four locations and by visually comparing the North American Regional Reanalysis dataset (NARR) along with modeled simulations. The most satisfactory scheme combination was

the WRF Single-Moment 3-class Microphysics scheme, Kain-Fritsch cumulus parameterization scheme and Yonsei University scheme for the planetary boundary layer. The planetary boundary layer schemes were noted to have the greatest influence in determining the most satisfactory model simulations. There was limited influence from different selections of microphysics and cumulus parameterization schemes. The preferred physics parameters from these simulations were then used in six additional simulations to analyze the affect different initialization data sets have with regards to model output. Data sets used in these simulations were the Final Operational Analysis global data, North American Regional Reanalysis (3 and 6 hour) and the North American Mesoscale Model at 1, 3 and 6 hour timesteps, for a total of six simulations. More timesteps or an increase in model resolution did not materially improve the model performance.

Chapter 1: Background and Event Overview

Deadly wintertime mesoscale severe weather events occur in the Ohio Valley more often during a La-Niña (cooler water temperatures in the tropical pacific over 0.5°C for a minimum three month period) similar to the 2008-2009 winter season (Rhome et al. 2000). La-Niña conditions usually correspond to warmer and wetter than normal temperatures over a given season in the Ohio Valley. A squall line of severe thunderstorms moved through the lower Ohio Valley on January 29-30, 2008. Two deaths occurred from wind damage and tornadoes. Another injury occurred as a result of large hail (Storm Data 2012). As a result, it is suggested that the understanding and prediction of these events is necessary. Meteorological models are a key tool for weather forecasters at any forecasting agency. These models require the use of physics parameterization schemes and model initialization data to run properly. Parameterization schemes simplify representations of complex physical processes within the atmosphere (Stensrud 2007). Initialization data sets provide the meteorological data used to start a model simulation. The purpose of this thesis was to examine the sensitivity of meteorological model output when these two critical model characteristics, parameterization schemes and initialization datasets were changed.

An examination of this meteorological event was completed through modeling of atmospheric conditions before, during and after this event. The Weather Research and Forecasting model version three (WRF) was used to conduct model simulations (Skamarock et al. 2008). A performance assessment of model data was completed through statistical analysis along with a visual comparison of observed and simulated atmospheric conditions.

1.1 MCS/Squall Line

Mesoscale Convective Systems (MCS) can be defined as complexes of thunderstorms which become organized on a scale larger than the individual thunderstorms, and normally persist for several hours (NWS 2012). A squall line is a form of a MCS, and defined as a narrow band of active thunderstorms (Newton 1950). The nature of these thunderstorm bands is often seen on radar displays as linear. In North America, these bands of thunderstorms often extend north to south, ahead of a surface frontal boundary due to linear nature of forcing in the atmosphere. If meteorological conditions are favorable, squall lines can be severe and destroy property and lives within a given area. Such squall lines affect the Ohio Valley frequently with high winds over 26 m/s, hail and isolated tornadoes (Wilson et al. 2009).

Certain conditions need to be met to develop and maintain a squall line. Squall lines can occur with a wide range of Convective Available Potential Energy (CAPE) and vertical wind shear (changing winds with direction or height) values. However, a squall line that has lower amounts of shear usually spreads out quicker and weakens since shear contributes to the organization of thunderstorms. Horizontal vorticity (change in direction or speed of wind on a horizontal axis) with squall lines is generated around individual cells causing upward motion (Meted 2012). A surface cold pool from the downdraft usually forms once a squall line produces rainfall which strengthens as new cells develop (Meted 2012). The cold pool circulation balances horizontal vorticity generated at the peak of squall line development. Once the cold pool strength is greater than the horizontal vorticity the cells become less intense since the upward motion is being cut off (Fig 1.1). Another element of a squall line, the rear-inflow jet (RIJ) forms

due to horizontal buoyancy gradients through front to rear (FTR) ascending current (Fig 1.1 and Fig 1.2). The strength of the RIJ is directly related to these gradients and stronger amounts of shear. A stronger FTR occurs when warmer air is transported aloft which enhances horizontal vorticity and the RIJ. The role of the RIJ is to entrain air from the mid-levels into a thunderstorm (Meted 2012). Often this movement of air can be fast leading to damaging winds and produces features such as shelf clouds (Fig 1.2).

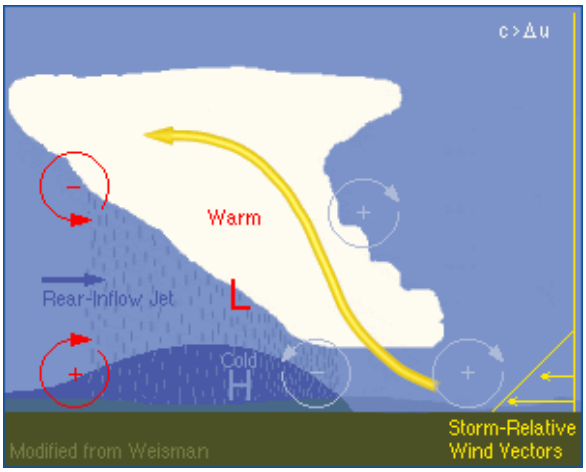

Fig 1.1. Diagram of a thunderstorm within a MCS or squall line. Warm air transport through the FDR(yellow line). Eddies of air transported shown with red and blue circles. Realtionship shown when the strength of the cold pool is greater than the amount of shear. RIJ and cold pool also shown.

Source: http://www.meted.ucar.edu/convectn/mcs/mcsweb/mcsframe.htm

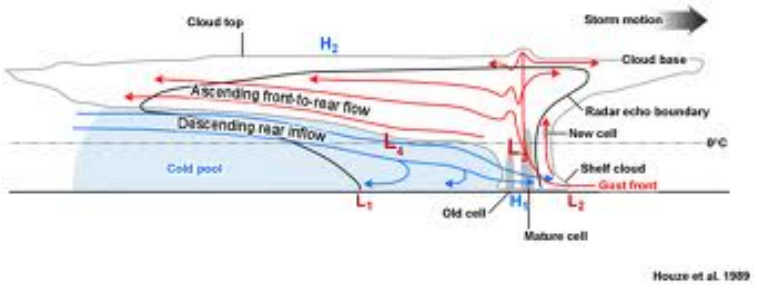

Fig 1.2. Diagram of a squall line showing cloud characteristics, cell delevopment and flow asscoiated with a typical squall line. The squall line is moving away from B and toward point A. Source: Houze et al. 1989

Squall lines are the most dominant severe weather mode east of the Mississippi River (Wilson et al. 2009). The challenge in forecasting these events lies with determining squall line strength, location and speed. Models, simulations of potential atmospheric conditions through numerical prediction are a key aid in determining these characteristics. Advanced warning due to improved modeling can mean the difference in life or death for some.

1.2. Squall Line Chronology

A noticeable temperature difference was present throughout Western and Central Kentucky from Murray to Liberty, KY with a temperature range from -15 °C to 15 °C along the frontal boundary from 18Z January 29, 2008 to 06Z January 30, 2008 due to a meridional polar jet. An intense jet streak with 125 knot winds was also was present at the 300 mb level. The Ohio Valley region was in the left exit position of the jet streak. This is where convergence usually takes place at the surface with a symmetric jet streak. However, the jet streak present in this research is rounding the base of a trough

originating from the subtropical jet and merging with the polar jet in a region of divergence (Fig. 1.3 and Fig. 1.4). Jet streaks are defined as regions within the jet stream that have stronger winds than the surrounding winds along the jet stream (strong winds concentrated in a narrow stream in the atmosphere) (NWS 2012). At other pressure levels height amplification due to the upper jet was present which resulted in considerable moisture and warm air advections. These features supplied a dynamical environment sufficient for the development of a squall line of thunderstorms with a strong west to southwest wind throughout the atmospheric column and a lack of instability compared to squall lines in warmer seasons (Fig. 1.3).

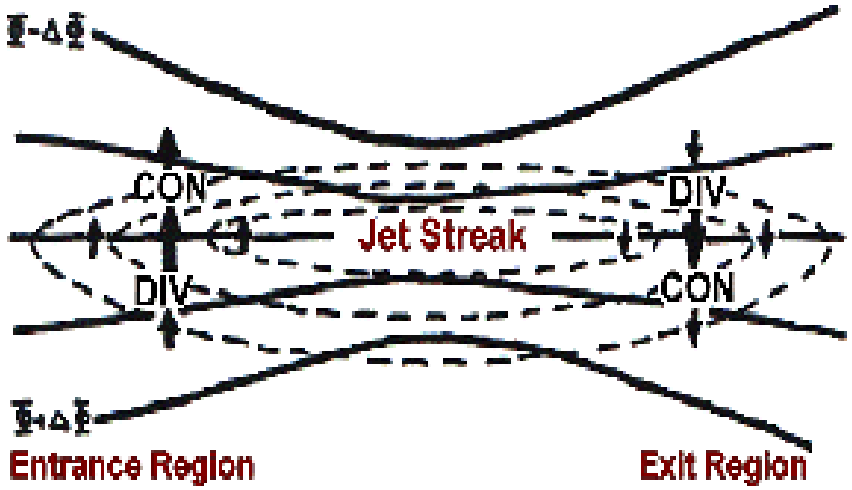

Fig. 1.3. Diagram of a jet streak, with entrance, exit regions along with regions of convergence and divergence. Solid black lines indicate height contors. Dashed lines indicate wind speed (isotachs).

Source: http://www.crh.noaa.gov/lmk/soo/docu/forcein.gif

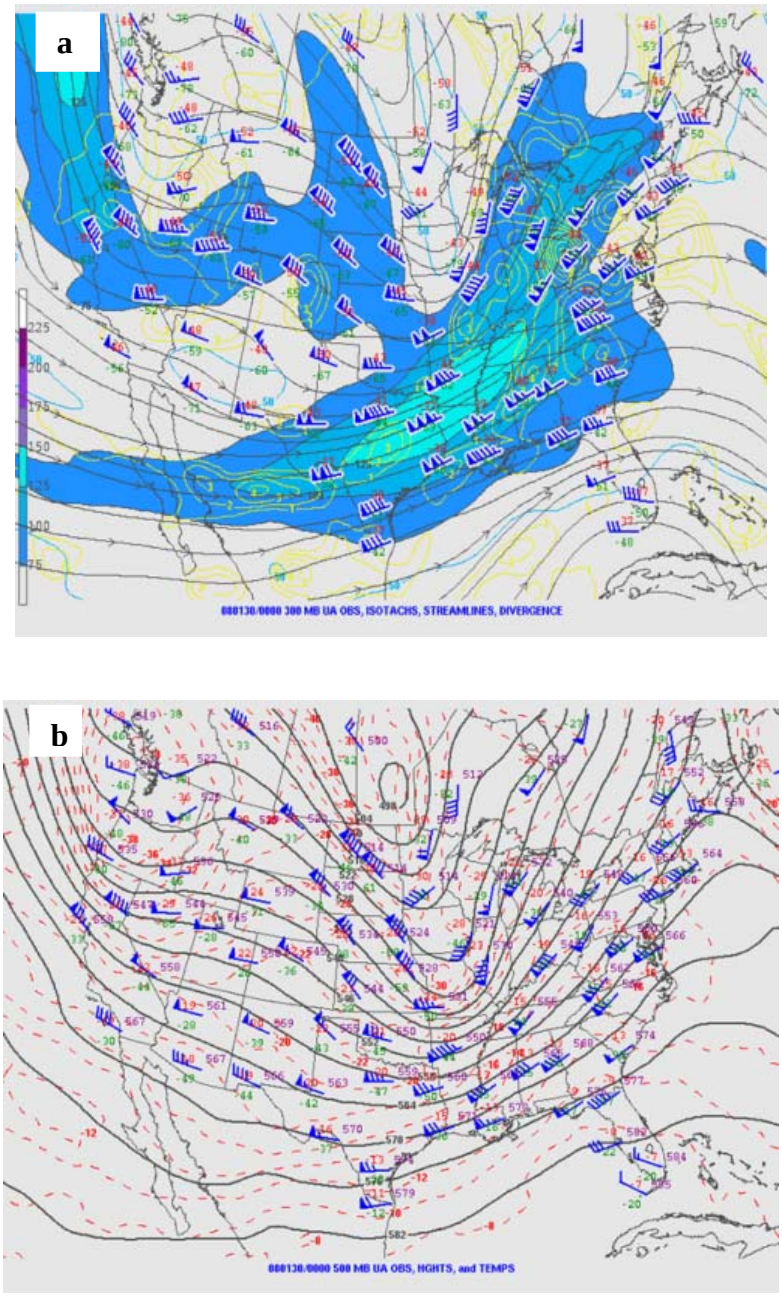

Fig. 1.4. January 29-30, 2008 squall line: a) 300 mb jet stream with range from (darkest blue) 75 knots to (lightest blue) 125 knots, and b) 500 mb height pattern with height lines in black. Source: www.spc.noaa.gov/exper/archive/080129/index.html

Squall line development began at approximately 2230Z on January 29 across southern Indiana and western Kentucky. This squall line, from 2230Z on January 29 to 0000Z on January 30, continued to develop into western Kentucky crossing the first Mesonet location at Murray by 0000Z (Fig. 1.6).

The Kentucky Mesonet is a state-wide environmental monitoring network which records meteorological variables at five minute intervals (Brown et al. 2009). This network has expanded from only a handful of Mesonet locations in 2008 (four inside the model domain at the time of this study) to 62 stations at present day (Mahmood 2012 personal communication) (Fig. 1.6). The passage of the squall line at Murray, KY corresponds to a change of maximum wind gusts between 2300Z and 0000Z. Wind gusts for the period ranged from 16 to 27 m/s. This was accompanied by a temperature drop from about 15 °C to 8 °C. Only 1.52 mm of rain fell with the passage of the squall line.

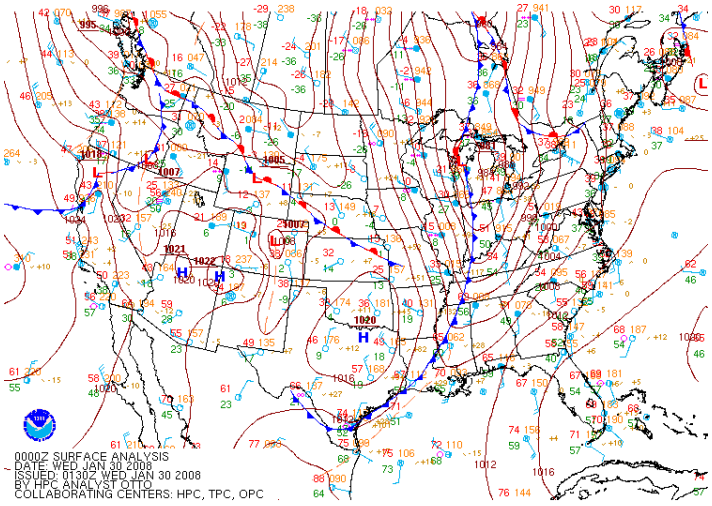

Fig. 1.5. National Oceanic and Atmospheric Administration (NOAA). Surface map from Jan 30, 2008 at 0000Z. Source: www.hpc.ncep.noaa.gov.

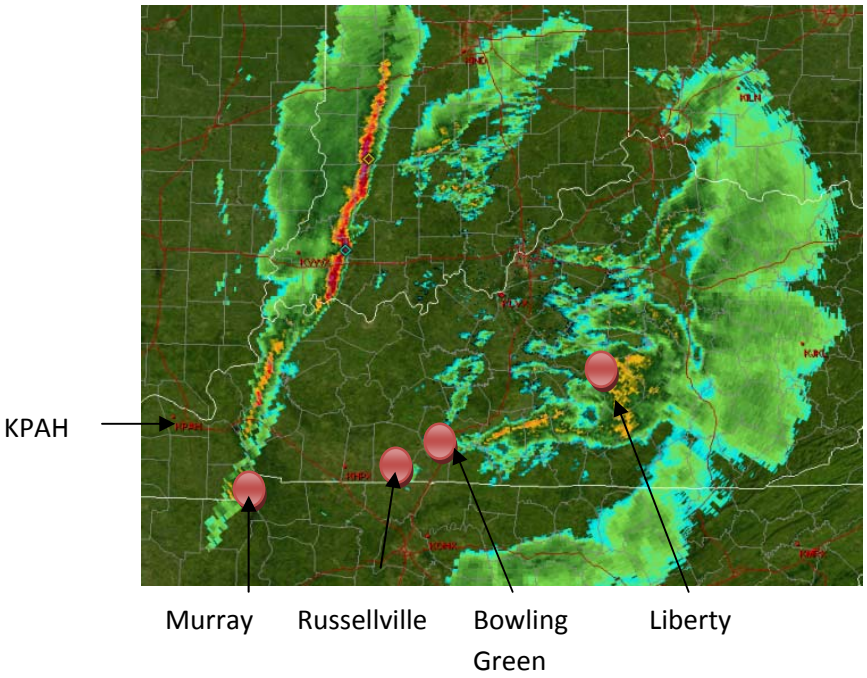

Fig. 1.6. Radar imagery for 2330Z on January 29, 2008 east of radar site KPAH (Paducah, KY).

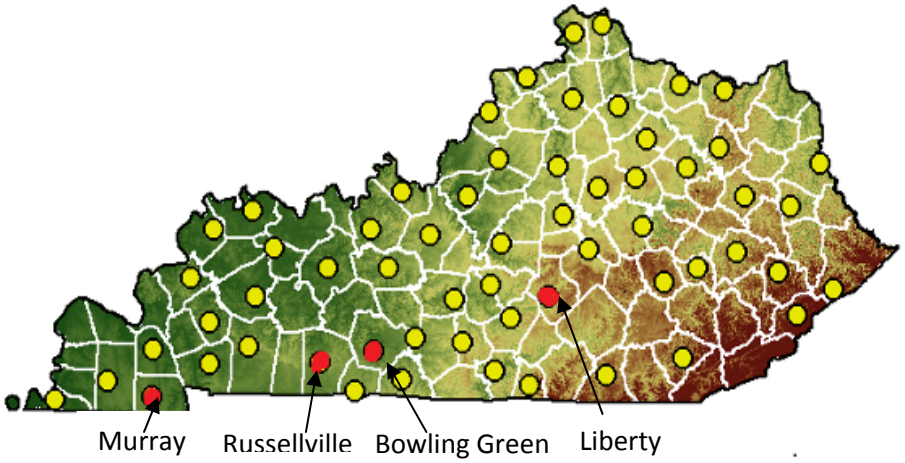

Fig. 1.7. Current Kentucky Mesonet locations, Kentucky Mesonet sites selected for this research in red. From west to east the locations are Murray, Russellville, Bowling Green and Liberty.

At the time the squall line moved through Russellville, between 0045Z and 0100Z on January 30, wind gusts increased from 8.94 m/s to 19.00 m/s with a sharp temperature drop from about 15 °C to 9 °C. By 0110Z on the January 30, the squall line had reached the Bowling Green Mesonet location (Fig. 1.7). Wind gusts increased from 13 to 23 m/s over a 20 minute period. By 0220Z, the squall line passed over the Liberty Mesonet location which corresponded to one of the higher wind gusts of 28 m/s. At the Bowling Green and Liberty Mesonet locations, rainfall amounts were just over one mm and the temperature decreased to about 5 °C with the passage of the cold front.

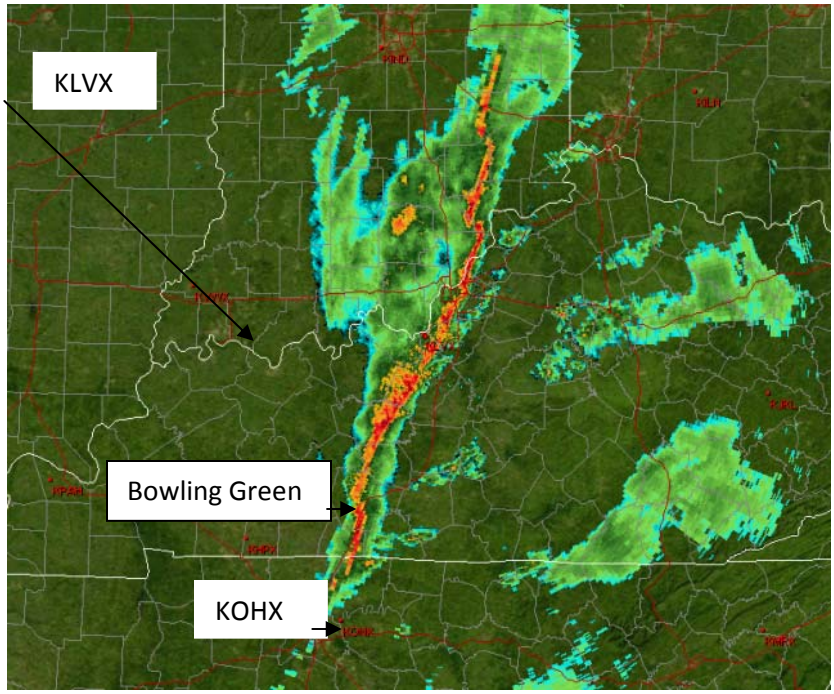

Fig. 1.8. Radar imagery for 0110Z on January 30, 2008 as the squall line passes over radar locations KOHX (Nashville, TN) and KLVX (Ft. Knox, KY).

Chapter 2: An Analysis of WRF Physics Parameterization Scheme Combinations for the January 29-30, 2008 Ohio Valley Squall Line Event

2.1 Meteorological Models

Models are useful tools to aid forecasters in determining characteristics of a variety of weather events. These models take an initial timeframe analysis of the atmosphere and attempt to predict the future state. To accomplish this, weather models use a series of mathematical equations to describe the changes of physical properties within the atmosphere and produce a simulation of atmospheric conditions. To forecast weather events several types of models are used by forecasters and researchers. Examples of models used in a research setting include the Regional Atmospheric Model System (RAMS) (Pielke et al. 1992) and the Weather Research and Forecasting model (WRF) (Skamarock et al. 2005).

Model simulations can predict conditions from a few hours in advance to even a week or two in advance with a wide range in the potential area that can be covered. Model domains can encompass the entire globe or a very small region such as Western Kentucky. The Global Forecast System (GFS) has the longest simulation time of any current model at 384 hours in advance and has a domain that encompasses the entire globe. The length of model simulations decreases with the North American Mesoscale Model (NAM) to 84 hours with coverage only over North America. WRF simulations usually are 24 to 36 hours in length from the initial start time with a regional coverage such as the Ohio Valley. Decreased simulation times and overall area can reflect a higher degree of a model's resolution both in terms of time intervals and resolution detail in the

simulation. The WRF simulations can achieve a simulation that has a high resolution over a small area relative to other models for a region of interest.

The WRF was used for the investigation of the squall line of January 2008. In order to generate a WRF model simulation, an initial dataset was used as a starting point from which a model simulation can be conducted. There are multiple datasets available for use in the WRF. The initial datasets served as a basis for the model to interpret the weather conditions at the start time of a simulation. Each initialization dataset had different characteristics that made them unique. These different sources of data for the WRF come with different time intervals. For the purposes of selection of parameterization scheme combinations, the North American Regional Reanalysis (NARR) dataset was used in 3-hour intervals. This data was pre-processed through the WRF pre-processing system (WPS) (Fig. 2.1). The WPS allowed for the interpretation of the incoming data. Actual modeling took place once the interpreted data reached the Advanced Research WRF (ARW). Within the ARW model, the selection of various physics schemes occurred. The final step in the modeling process was visualization and verification of data. These steps can be seen below through use of a flow chart (Fig. 2.1).

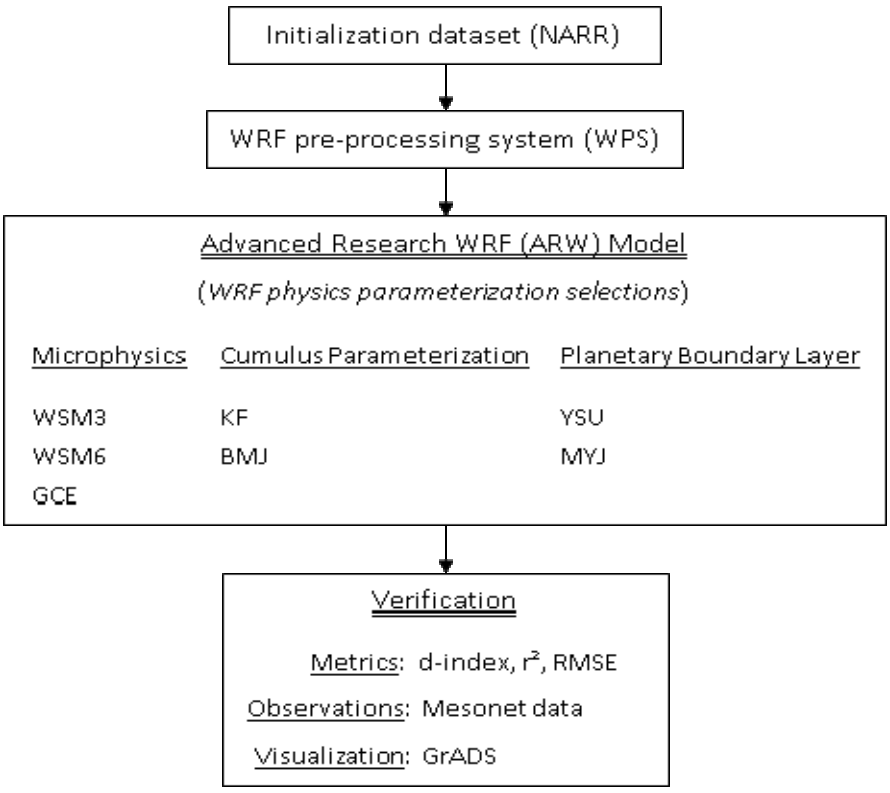

Fig. 2.1. Flow chart describing WRF simulations from data entry to visualization.

Through use of the WRF, sensitivity tests were conducted to measure the accuracy of model results generated using different combinations of physics parameterization schemes. Each physics parameterization scheme used different mathematical equations that governed atmospheric motion within the model that influenced simulations. Various combinations of physics parameterization schemes within the WRF for the squall line event in question were compared in order to determine which scheme combinations were satisfactory representations of the event. This was completed through statistical and visual analysis of model data.

2.2. Overview of Parameterization Schemes

There are several cloud microphysics parameterization schemes that can be used in WRF-based experiments. Microphysics (MP) is the study of cloud formation and cloud particles including ice water and nuclei. In this case, the different microphysics parameterization schemes examine how these particles will interact as well as how they grow into precipitation particles in the atmosphere over time. The three microphysics parameterization schemes, that were used and analyzed, included the single-moment 3 and 6-class Microphysics Schemes (WSM3 & WSM6) (Lin et al. 1983; Dudhia 1989; Hong and Lim 2006) and the Goddard Cumulus Ensemble model (GCE) (Rutledge and Hobbs 1984; Mccumber 1991: and Tao 2003).

The Thompson MP scheme (Thompson et al. 2004) was a scheme which focused on six classes of microphysics selections. The WSM5, which only differed from the WSM6 in the classification of graupel, was not used (Hong et al. 2004). The Lin and Kessler schemes (Lin et al. 1983; Kessler et al. 2006; and Rutledge and Hobbs 1984) were not incorporated as well since they are simpler schemes with fewer classifications. These schemes were not cited as frequently in prior studies. Basic assumptions of the WSM3 and WSM6 are that ice phase processes primarily occur between 0 °C and -20 °C. Rain processes occur for temperatures above freezing. Snow processes occur for temperatures below freezing. Ice crystal concentration is a function of ice amount (Dudhia 1989 and Hong et al. 2004). These basic assumptions allow for a better distribution of cloud ice and snow concentrations. A primary difference between

the WSM3 and WSM6 is the representation of different water forms including: vapor, cloud water, cloud ice, rain, snow and hail (Lin et al. 1983). The WSM6 expands the number of arrays to individually classify each of these six categories from the WSM3. However, improvements with the WSM6 have been most noted on cloud resolving grids (Hong and Lim 2006).

The Goddard (GCE) microphysics scheme employs similar class schemes to the WSM microphysics parameterization schemes with six different classifications (Lin, 1983). The formation of this MP scheme is independent of relative humidity as well, which causes ice to be converted to snow even with subsaturation (Tao et al. 2003).

Two planetary boundary layer (PBL) schemes, namely the Yonsei University Scheme (YSU) (Hong and Kim 2007) and the Mellor-Yamada Janjic (MYJ) (Hong et al.2006; and Janjic 1990) are available for WRF simulations. PBL schemes involve boundary layer fluxes, vertical diffusion, heat flux and frictional forces within the atmosphere. They also measure the mixing of air between layers of the atmosphere (Hong and Kim 2007). The YSU parameterization scheme is a revised vertical diffusion package with a nonlocal turbulent mixing coefficient (Hong and Kim 2007). This scheme also allows for the depth of the PBL to be determined from the thermal profile and a mixing scheme in the boundary layers. This scheme is based on a simple nonlocal-K approach and its ability to utilize large-eddy simulation (Hong and Pan 1996). It also features the inclusion of an explicit treatment of entrainment at the top of the PBL. This entrainment process leaves more heat and moisture for the accurate representation of severe convection (Hong et al. 2006). On the other hand, the MYJ scheme involves higher order

closure approaches (Hong et al. 2006 and Janjic 1990). Higher order closure approaches parameterize the change in mean potential temperature over time. This scheme is also defined as a local diffusion scheme. In a local diffusion scheme the mean potential temperature of the PBL depends only on a given altitude. This assumes only small eddies are present within the PBL. Local diffusion schemes have a strong tendency to underdevelop convection due to a strong capping inversion (Ayotee et al. 1996).

In addition to the PBL and microphysics parameters, there are several cumulus parameterizations (CP) schemes that can be used in the WRF model. CP schemes involve updrafts, downdrafts, entrainment of air and detrainment of air throughout the height of the atmosphere, including the boundary layer. Two CP schemes that were investigated include the Kain-Fritsch (KF) (Kain and Fritsch 1990) and Bets- Miller-Janjic (BMJ) (Betts, 1986; and Betts and Miller 1986). The Grell-Devenyi scheme (Grell and Devenyi 2002) was not used since the primary focus of this scheme was ensemble research. Simulations with no CP schemes were not conducted. Etherton and Santos (2008) noted that in several cases having no CP scheme in place resulted in extreme amounts of convection produced by WRF.

Kain-Fritsch uses a simple cloud model with updrafts and downdrafts which include the effects of detrainment and entrainment (Kain and Fritsch 1990). A two-way exchange of mass between clouds and the surrounding environment at each vertical level occurs by a buoyancy sorting mechanism. This allowed for the realistic simulation of vertical profiles both in terms of updraft moisture detrainment and mass flux in a two-dimensional setting (Kain and Fritsch 1990) This also can be extended to the representation of a minimum entrainment rate to represent dry conditions and vary as a

function of low-level convergence (Kain 2004). The Bets-Miller-Janjic (Betts 1986; and Betts and Miller 1986) has deep and shallow profiles with no explicit updrafts and downdrafts along with a saturated profile. This scheme was based on the Betts scheme but has an additional deep convection algorithm to define the moisture profile (Betts 1986; and Betts and Miller 1986). Cloud efficiency is proportional to combination of entropy and precipitation change over time. The base value of the entropy change is set to a region where convection does not develop. In addition, this scheme is based on the work of the buoyancy force on an ascending parcel reaching a prescribed level in the atmosphere (Skamarock et al. 2005).

Several studies have examined the accuracy of WRF simulations by using different parameterization schemes (Jankov et al. 2005; Gallus and Bresch 2006; Weisman et al. 2008; Hu et al. 2010; Rajeevan et al. 2010; Ruiz et al. 2010; and Schwartz et al. 2010). Changing parameterization schemes can show differences or similarities in some aspects of model simulations (Jankov et al. 2005; Gallus and Bresch 2006; Rao et al. 2007; Weisman et al. 2008; Hu et al. 2010; Rajeevan et al. 2010; and Ruiz et al. 2010).

Parameterization schemes used with regards to model ensembles can also be examined (Eckel and Mass 2005; Schwartz et al. 2010; and Tapiador et al. 2012). An ensemble is the same model run many times to gauge a sample of model data.

These studies also have had some notable findings regarding the selection of physics parameterization schemes. Jankov et al. (2005) cited the selection of the KF CP scheme as opposed to the BMJ which produced lighter, widespread amounts of precipitation and decreased the maximum precipitation amounts. Weisman et al. (2008) discussed the YSU PBL created boundary layers that are deeper and drier. As a result,

capping inversions can be easier for the model to remove. Weisman et al. (2008) then compared this to the MYJ scheme, which tends to slowly deepen the boundary layer. This can result in PBL conditions that are cooler with stronger caps. Taipador et al. (2012) also noted in his study that only a minimal difference was present between the WSM MP selections.

The purpose of this thesis was to determine which combination or combinations of these parameterization schemes discussed above had the most satisfactory modeling results for a squall line which passed through the region on January 29-30, 2008. The analysis of these schemes and scheme selection showed that physical differences do exist between the schemes and these scheme differences may affect model results.

2.3. Experimental Design

Three WRF models domains were used. The inner domain had a resolution of 1 km and primarily represented western and central Kentucky. Higher resolutions were used in this study because of the localized nature of the event in question and the desire for detailed simulations over the Mesonet locations. The finer model resolution allows for the simulations to detect a majority of mesoscale features within the inner domains (Weisman et al. 1997).The middle domain has a resolution of 3 km which covers a larger region of the Ohio and Tennessee Valleys along with portions of the southern US (Fig. 2.2). The outer domain (9 km resolution) covers most of the eastern US including the Great Plains.

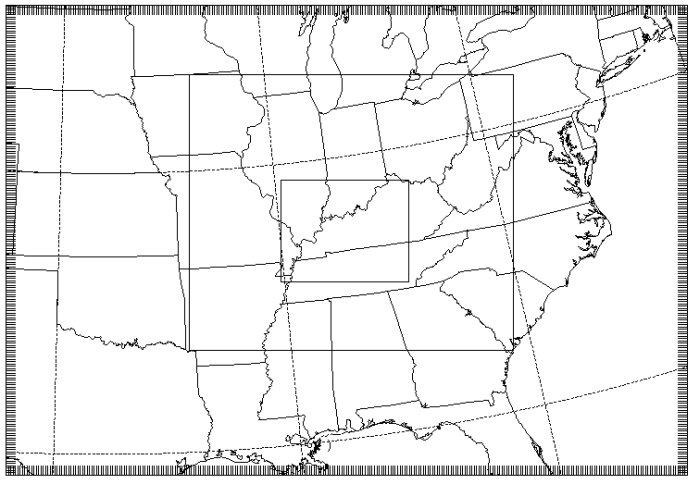

Fig. 2.2. Layout of model domains. Domain 1 showed model output for the central and eastern US with 9 km resolution. Domain 2 spanned the Ohio Valley and mid-south with 3 km resolution. Domain 3 showed model output for the central and western Kentucky with 1 km resolution.

As noted before, NARR data with 3-hour intervals was used. NARR is a long-term, consistent, high-resolution climate dataset for the period of 1979 through present day (Mesinger et al. 2006). However, the NARR dataset has several unique characteristics to differentiate it from other datasets. NARR has a resolution of 32 km with 45 vertical layers. Another key difference is the use of the older Eta physics package. NARR also features a fully cycled assimilation system. This system allows for the generation of a first guess for the next 3-hour block of data. Precipitation is assimilated which allows for the conversion of latent heat. The updated technique has been shown to affect temperature and precipitation (Mesinger et al. 2006). For temperatures, the majority of data comes from radiosondes. After completion of each WRF run, a point validation program was used. This program records the WRF model

output with selected geographical coordinates for a particular location. These locations can then be matched up with the locations of the Mesonet sites for the model output data.

Model output data were then verified with the Kentucky Mesonet surface observations. Verification would show if a model simulation was a satisfactory interpretation of an atmospheric event. The source for observed surface data was the Kentucky Mesonet as discussed in Chapter One. The Kentucky Mesonet surface data at five minute intervals was used to compare surface and model data. Model data was also used at five minute intervals with 144 data points for a 12-hour simulation for each Mesonet location. This high temporal resolution was a limiting factor in the use of other sets of meteorological data. The Automated Surface Observing System (ASOS) only produces data on average every 30 minutes, which would not be a temporal match. The higher temporal resolution gives more detail into the timing of the weather changes. Figures were created for comparisons among different simulations and observations through use of the grid analysis and display system (GrADS), (Institute of Global Environment and Society 2011). With regards to the length of each simulation, the timeframe was 1200Z on the 29th through 1200Z on the 30th. This timeframe included 12 hours of spin-up time, before the main squall line passed through the lower Ohio Valley at the center of the model domain, and about 12 hours following the evolution of the squall line. The spin-up time is the time needed for the model to account for the weather patterns and conditions.

Model performance analyses were completed for each set of model data to compare the different simulations with a specific combination of parameterization schemes. Statistical measures of r^2, RMSE, and an index of agreement "(*d-index*)" were

used (Legates and McCabe 1999). The r^2 statistic is defined as the square of the Pearson product-moment coefficient, while the RMSE is the square root of the mean square error. For r^2, values near one indicate a strong positive correlation while values near zero indicate no correlation. A similar scale is used for the *d-index* from zero to one with one indicating a higher agreement in any data analyzed. The RMSE describes the amount of error in terms of the variable and quantifies it. For example, the amount of temperature error would be in degrees Celsius and a higher RMSE would mean a larger error. It should be noted that the r^2 and RMSE measures have been known to produce a biased view of model efficiency. The primary reason for this is the sensitivity of the squared values which tend to allow outliers to have more influence. These measures are also oversensitive to extreme values and insensitive to additive differences between model predictions and observed data (legates and McCabe 1999). The reasoning noted above explains why three statistical measures were used to best gauge any potential bias. Additional time series and graphics were created to give a visual reference for comparison of model data in terms of schemes used and to compute statistical values between modeled and Mesonet values for each variable. Figures were prepared to show the distribution of precipitation with NARR as a reference.

2.4. Results

Modeled and observed temperature, precipitation, relative humidity, and dewpoint temperature data from the Mesonet were analyzed for Murray, Russellville, Bowling Green and Liberty. At Murray, inclusion of the YSU PBL produced higher r^2, lower RMSE and higher *d-index* results in all 18 occurrences for temperature and dewpoint temperature, 16 of 17 occurrences for precipitation and 17 of 18 occurrences for relative

humidity (RH) (Table 2.1). Within the tables, bolded indices indicate higher *d-index* and r^2 values along with lower RMSE values. An occurrence can be broken down by variable and parameterization scheme. For example, with the PBL six comparisons can be made for *d-index*, r^2, and RMSE with each PBL scheme given no change in MP and CP schemes were made. With regards to the CP analysis, inclusion of the BMJ selection produced superior results in most cases for temperature, precipitation and RH, while for dewpoint temperature the BMJ and KF schemes produced similar results. Inclusion of the YSU PBL scheme with other CP and MP schemes also produced statistically superior results in Russellville (Table 2.2). Of the possible 18 performance assessments and their statistics, 16 found that inclusion of the YSU PBL scheme produced superior results for temperature. Superior results were also obtained with 16 of 17 performance assessments for RH and 15 of 16 for dewpoint temperature. In terms of CP and MP, inclusion of the KF CU and WSM3 MP also produced superior results.

There were fewer differences in terms of CP and MP combinations at Bowling Green. With reference to temperature, three of six combinations for CP schemes produced a *d-index* value that only differed based on PBL scheme. Two of the other three produced a slight preference toward the BMJ scheme. The WSM3 MP had a higher *d-index* and lower RMSE in four of six model simulations that analyzed the difference in MP combinations. The r^2 values were all, however, influenced more by the PBL schemes than the MP or CP schemes.

In terms of precipitation and relative humidity at Bowling Green, a comparison of all YSU PBL schemes showed varying results with regards to MP and CP scheme selections. In terms of *d-index* for precipitation, inclusion of the KF scheme produced

higher values for all three potential combinations with YSU. Inclusion of the KF scheme also produced lower RMSE values compared to scheme combinations with the MYJ PBL. For relative humidity, the *d-index* values were similar among the MP schemes. When examining CP schemes, the KF has a lower RMSE in two of three potential scheme combinations.

It was found that at Bowling Green, the inclusion of the YSU PBL scheme produced a higher *d-index* value on 20 of the 24 combinations for precipitation, relative humidity, dewpoint and surface temperature (Table 2.3). For temperature, inclusion of YSU produced RMSE values close to 1.60 °C for four out of six simulations. Moreover, selection of MP and CP schemes with the YSU PBL produced higher r^2 values between 0.97 and 0.99 for temperature.

Results for Liberty (Table 2.4) showed that inclusion of the YSU PBL produced higher *d-index* and r^2 and lower RMSE values in the majority of combinations. However, the inclusion of both CP and MP schemes did not produce notable differences in the quality of model simulations. Inclusion of the WSM3 MP produced more satisfactory results for five of 12 potential combinations. It was more than each of the other potential MP selections but not with an overwhelming superiority.

Table 2.1. Performance of combinations of parameterization schemes between modeled and Kentucky Mesonet data for Murray, KY. (Bolded statistics indicate values that are the most satisfactory for performance evaluation for each near surface atmospheric variable).

			Temperature			Precipitation			Relative Humidity			Dewpoint Temperature		
MP	CP	BL	*d-index*	r^2	RMSE (°C)	*d-index*	r^2	RMSE (mm)	*d-index*	r^2	RMSE(%)	*d-index*	r^2	RMSE (°C)
WSM6	KF	MYJ	0.65	0.91	6.17	0.19	0.66	12.20	0.98	0.53	9.98	0.69	0.89	6.97
		YSU	0.90	**0.97**	4.09	0.34	**0.75**	9.23	0.83	0.76	8.35	0.94	**0.96**	3.45
	BMJ	MYJ	0.62	0.92	5.81	0.17	0.68	12.40	0.80	0.54	9.72	0.75	0.90	6.51
		YSU	0.91	0.94	4.12	0.59	0.70	6.02	0.90	0.81	8.00	**0.97**	0.95	3.53
WSM3	KF	MYJ	0.69	0.89	6.10	0.28	0.64	12.37	0.81	0.50	9.67	0.81	0.87	6.96
		YSU	0.88	**0.97**	4.00	0.41	0.73	8.24	0.84	0.73	7.90	0.94	0.95	3.68
	BMJ	MYJ	0.68	0.89	6.18	0.76	0.62	12.19	0.81	0.50	9.72	0.80	0.88	7.06
		YSU	**0.94**	0.93	**3.78**	0.38	0.62	**5.64**	**0.99**	0.70	**7.84**	0.95	0.95	**3.23**
GCE	KF	MYJ	0.53	0.90	6.30	0.16	0.61	12.80	0.77	0.56	9.56	0.68	0.89	7.10
		YSU	0.92	0.94	4.12	0.45	0.67	8.15	**0.99**	0.75	8.97	**0.97**	**0.96**	3.41
	BMJ	MYJ	0.53	0.91	6.31	0.15	0.68	13.00	0.81	**0.85**	8.95	0.71	0.90	6.85
		YSU	0.92	**0.97**	3.95	**0.61**	0.70	5.66	0.87	0.76	8.53	**0.97**	**0.96**	3.37

Table 2.2. Performance of combinations of parameterization schemes between modeled and Kentucky Mesonet data for Russellville, KY. (Bolded statistics indicate values that are the most satisfactory for performance evaluation for each near surface atmospheric variable.)

			Temperature		Precipitation				Relative Humidity			Dewpoint Temperature		
MP	CP	BL	*d-index*	r^2	RMSE (°C)	*d-index*	r^2	RMSE (mm)	*d-index*	r^2	RMSE (%)	*d-index*	r^2	RMSE (°C)
WSM6	KF	MYJ	0.73	0.86	4.92	0.90	0.92	7.69	0.59	0.70	10.22	0.68	0.90	6.29
		YSU	**0.99**	0.98	2.59	0.86	0.71	**3.87**	0.85	0.73	7.94	0.96	**0.98**	2.99
	BMJ	MYJ	0.78	0.87	4.06	0.92	**0.95**	6.39	0.60	0.68	10.43	0.72	0.91	5.99
		YSU	0.94	0.86	4.93	0.63	0.94	6.26	0.77	0.67	10.52	0.72	0.90	6.36
WSM3	KF	MYJ	0.76	0.86	4.92	0.58	0.94	6.26	0.74	0.67	10.51	0.80	0.90	6.36
		YSU	0.97	0.98	**2.39**	**0.97**	0.70	4.22	0.81	0.69	7.99	0.96	0.97	**2.61**
	BMJ	MYJ	0.94	0.86	4.88	0.71	**0.95**	5.18	0.74	0.61	11.00	0.76	0.90	6.38
		YSU	0.98	0.97	4.93	0.81	0.67	6.26	0.82	0.69	10.52	0.94	0.96	6.36
GCE	KF	MYJ	0.72	0.84	5.01	0.89	0.94	7.98	0.54	0.66	10.71	0.66	0.89	6.50
		YSU	0.96	0.98	2.60	0.79	0.69	4.46	0.84	0.68	8.36	0.97	**0.98**	2.91
	BMJ	MYJ	0.82	0.85	4.93	0.89	0.94	8.10	0.56	0.71	10.48	0.67	0.91	6.39
		YSU	0.96	**0.99**	2.52	0.69	0.07	5.18	**0.89**	**0.80**	**7.84**	**0.98**	**0.98**	**2.61**

Table 2.3. Performance of combinations of parameterization schemes between modeled and Kentucky Mesonet data for Bowling Green, KY. (Bolded statistics indicate values that are the most satisfactory for performance evaluation for each near surface atmospheric variable.)

MP	CP	BL	Temperature			Precipitation			Relative Humidity			Dewpoint Temperature		
			d-index	r^2	RMSE (°C)	*d-index*	r^2	RMSE (mm)	*d-index*	r^2	RMSE (%)	*d-index*	r^2	RMSE (°C)
WSM6	KF	MYJ	0.67	0.85	4.17	0.67	0.97	10.18	0.54	0.55	10.64	0.68	0.91	5.45
		YSU	0.98	0.98	3.87	0.72	0.66	7.25	**0.85**	0.69	**8.01**	0.99	0.97	1.58
	BMJ	MYJ	0.72	0.88	3.83	0.72	0.88	**3.83**	0.70	0.54	10.56	0.79	0.92	5.05
		YSU	0.99	0.98	1.73	0.63	0.71	9.10	0.84	0.68	8.26	0.99	0.97	1.68
WSM3	KF	MYJ	0.95	0.87	4.07	0.95	0.97	9.11	0.71	0.54	11.16	0.78	0.92	5.50
		YSU	0.97	0.98	1.66	**0.97**	0.65	6.23	0.72	0.59	8.49	0.98	**0.98**	1.74
	BMJ	MYJ	0.95	0.87	4.10	0.68	0.96	8.06	0.69	0.53	11.43	0.77	0.92	5.59
		YSU	0.77	0.98	3.98	0.77	**0.98**	3.98	0.66	0.67	11.07	0.83	**0.98**	5.39
GCE	KF	MYJ	0.67	0.87	4.14	0.67	0.87	4.14	0.49	0.58	10.75	0.67	0.91	5.54
		YSU	0.98	0.98	1.64	0.72	0.66	7.43	**0.85**	**0.73**	8.05	0.99	0.97	**1.53**
	BMJ	MYJ	0.67	0.86	4.21	0.90	0.96	11.69	0.54	0.62	10.29	0.68	0.92	5.52
		YSU	**0.99**	**0.99**	**1.59**	0.54	0.80	10.96	**0.85**	**0.73**	8.03	**0.99**	0.97	1.54

Table 2.4. Performance of combinations of parameterization schemes between modeled and Kentucky Mesonet Data for Liberty, KY. (Bolded statistics indicate values that are the most satisfactory for performance evaluation for each near surface atmospheric variable.)

			Temperature			Precipitation			Relative humidity			Dewpoint temperature		
MP	CP	BL	*d-index*	r^2	RMSE (°C)	*d-index*	r^2	RMSE (mm)	*d-index*	r^2	RMSE (%)	*d-index*	r^2	RMSE (°C)
WSM6	KF	MYJ	0.66	0.73	3.74	0.81	0.97	8.75	0.69	0.43	7.08	0.71	0.72	4.25
		YSU	0.90	0.87	2.77	0.86	0.74	8.30	0.70	0.38	8.87	0.97	**0.96**	1.75
	BMJ	MYJ	0.73	0.76	3.50	0.76	**0.96**	9.88	0.74	0.43	**6.82**	0.79	0.75	3.82
		YSU	0.91	0.89	2.70	0.66	0.86	12.80	0.68	0.37	8.70	0.97	0.90	1.92
WSM3	KF	MYJ	0.69	0.76	3.60	0.58	**0.96**	8.93	0.74	0.38	9.02	0.73	0.73	4.18
		YSU	**0.96**	0.89	2.75	**0.92**	0.78	8.80	**0.99**	0.41	8.97	**0.98**	0.91	1.78
	BMJ	MYJ	0.69	0.75	3.61	0.84	**0.96**	7.73	0.73	0.45	6.86	0.76	0.74	4.03
		YSU	0.69	0.76	3.62	0.79	**0.96**	9.02	0.65	0.38	7.39	0.73	0.73	4.20
GCE	KF	MYJ	0.68	0.76	3.62	0.78	0.94	9.29	0.75	0.52	6.40	0.75	0.75	4.01
		YSU	0.92	**0.90**	2.69	0.83	0.81	8.73	0.75	0.59	8.69	**0.98**	0.91	1.59
	BMJ	MYJ	0.68	0.77	3.62	0.84	**0.96**	**7.67**	0.67	0.45	6.95	0.73	0.76	4.14
		YSU	0.92	**0.90**	**2.60**	0.69	0.90	12.03	0.75	**0.64**	8.81	**0.98**	**0.96**	**1.51**

The preference of the scheme combinations was also observed through an analysis of time series data with regards to each of the variables at the Mesonet locations (Fig. 2.3). Overall, the figures showed that the modeled and Mesonet data corresponded satisfactorily at all locations. In the model data, precipitation lagged a few hours, and was consistent throughout all the modeled simulations. However, even with this modeled lag, the overall total precipitation for the event at Bowling Green was 3 mm higher compared to the preferred scheme combination. Modeled temperature data showed notable agreement with observed data during the passage of the front (Fig. 2.3a) while modeled dewpoint temperature data showed systematic bias during this time period (Fig. 2.3b). The largest difference between the modeled and Mesonet dewpoint temperature values was about 3°C (Fig. 2.3b).

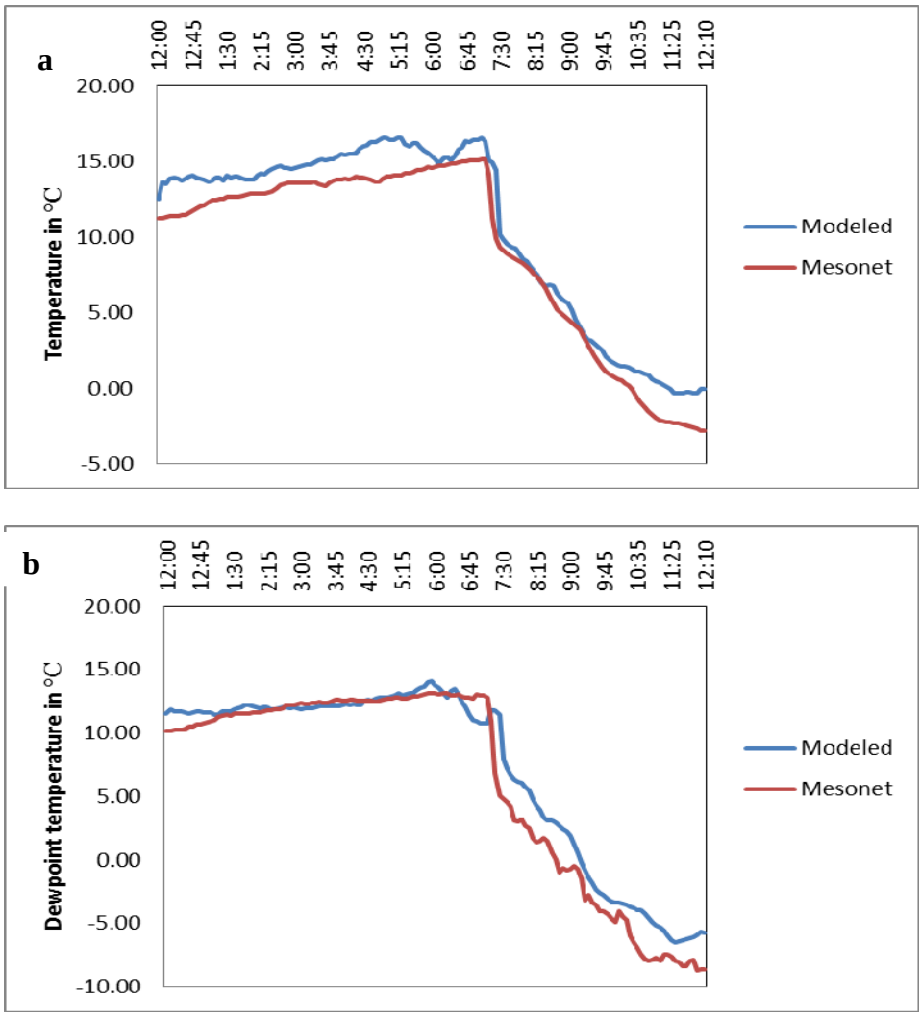

Fig. 2.3. Comparison of modeled and Mesonet data for Bowling Green, KY: a) temperature, and b) dewpoint temperature. The modeled data is from the preferred scheme combination WSM3_KF_YSU at 0000Z Janurary 30, 2008.

The findings at the four Mesonet locations agreed with previous research. Hong et al. (2006) suggested that the entrainment process left more heat and moisture for the accurate representation of severe convection with the YSU PBL. Ayotee (1996) and Hu et al. (2010) noted that local diffusion schemes such as the MYJ have a strong tendency to under develop convection due to a strong capping inversion.

Another key factor with regard to the PBL in model simulations was its respective height. PBL height plays a role in the formation of cumulus convection (Shin and Ha 2007). A PBL height that is too deep may have too much mixing and not accurately represent convection (Sanjay 2002). The MYJ scheme uses the turbulent kinetic energy profile to determine PBL height. On the other hand, the YSU scheme uses the bulk Richardson number to define the top of the PBL (Hu et al. 2010). They have also found that heights peaked early with model simulations using the MYJ PBL, suggesting less in the way of an entrainment processes.

A comparison of NARR data with modeled simulations also showed that the inclusion of the YSU PBL resulted in a more satisfactory temperature simulation of this squall line event when simulations using the MYJ PBL were compared (Fig. 2.4a-d). The use of the MYJ PBL scheme resulted in a more generic spread in temperature compared to the NARR temperature output and simulations with the YSU PBL. The overall spread in temperature on the NARR image ranges from -5 °C to almost 20 °C. The spread was only about 10 °C with modeled simulations using the MYJ PBL compared to the observed 25 °C with the NARR data. With the WSM6_KF_MYJ, simulated temperatures ahead of the cold front ranged from 10-15 °C. Behind the front, temperatures only slightly cooled to just under 10 °C (Fig. 2.4a-d). Even with a different selection of MP and CP schemes, the overall temperature difference between modeled simulations was not as sensitive as inclusion of different PBL schemes.

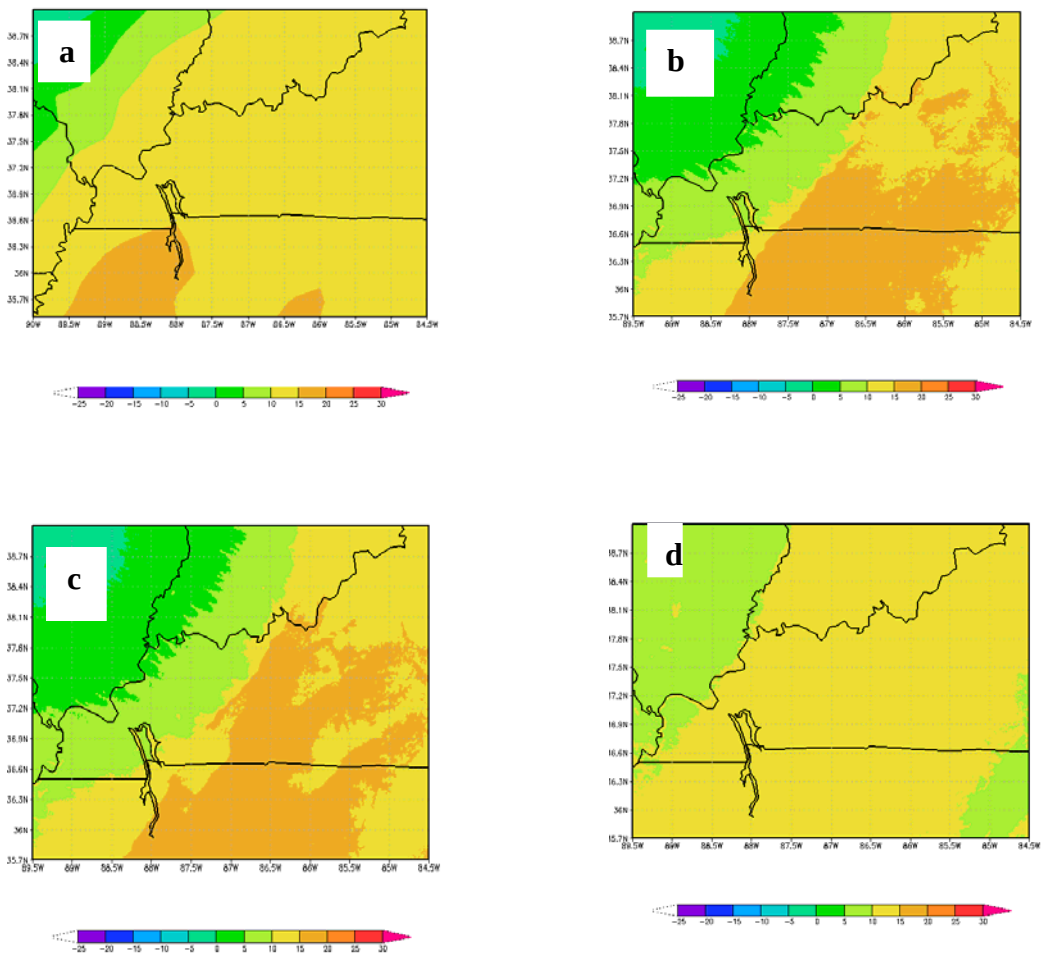

Fig. 2.4. Modeled surface temperatures in °C at 0000Z January 30, 2008: a) NARR, b) WSM6_KF_YSU c) GCE_BMJ_YSU, and d) WSM6_KF_MYJ.

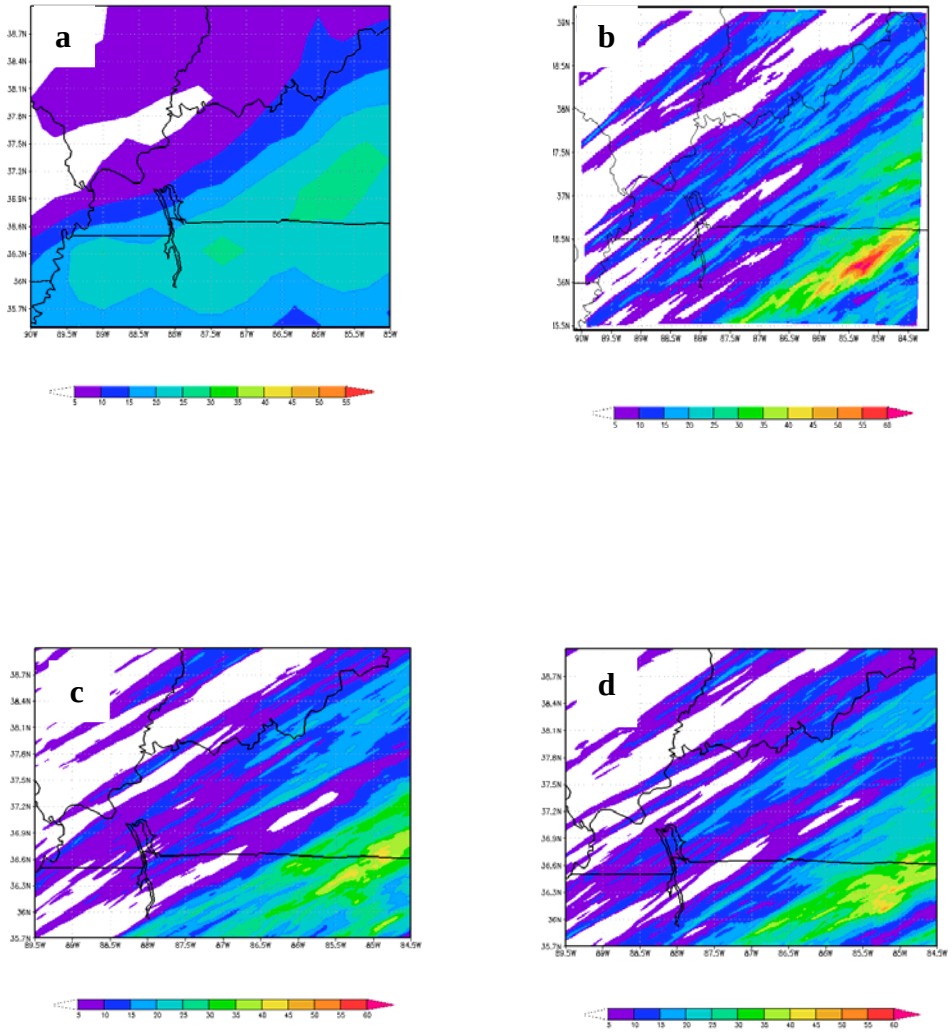

Fig. 2.5. Total precipitation for January 29, 2008 1200Z to January 30, 2008, 1200Z: a) NARR, b) WSM6_BMJ_YSU, c) GCE_KF_MYJ, and d) GCE_KF_YSU.

Simulations using the YSU PBL were able to define regions of precipitation over five mm in the southern Illinois/Ohio River Valley and Indiana. Model simulations with the YSU PBL also produced 10 mm precipitation amounts along the Ohio River which closely resembles the NARR representation (Fig. 2.5a-d). Of greater interest was that this group of model simulations produced more accurate precipitation totals over the Mesonet locations in south central Kentucky. The MYJ PBL model simulations produced very light precipitation, under five mm, over the region of interest. This difference in precipitation totals, when comparing PBL schemes, is likely due to the timing of development in precipitation. The MYJ PBL was not as satisfactory of a parameterization scheme for several reasons. This parameterization scheme was a local diffusion scheme that used higher order closure approaches and did not produce a favorable environment for entrainment (Ayotee et al. 1996; and Hong et al. 2006).

All of the model simulations had a southeast displacement due to convective feedback issues over Tennessee. In addition, the change in any scheme selection played a role in the location of precipitation anomalies. This phenomenon was observed by Rajeevan et al. (2010) who was able to determine that different microphysics schemes have a bearing on precipitation distribution. Jankov et al. (2005) found that the BMJ scheme produced too much widespread light precipitation, while the KF scheme produced more defined regions of rainfall (Jankov et al. 2005). Tapiador et al. (2012) suggested that this may be due to more grid-resolved precipitation with the KF scheme. In cases with the WSM schemes this appeared to have some influence. However, with the GCE MP few differences were noted between the CP schemes. More grid resolved

precipitation would result in better depictions of structure and heavy rain totals. The BMJ scheme eliminates conditional instability by adjusting temperature and specific humidity. If the atmosphere is not moist enough the scheme does not turn on. A bias of the scheme is to remove all available moisture (Gallus 1999). Weisman et al. (2008) also noted that microphysics selection did not contribute to or prevent errors in forecast guidance. Tapiador et al. (2012) noted that limited differences while comparing WSM schemes. These findings regarding the MP schemes carried over to this research.

Similarities in model simulations with regards to the MP and CP schemes were noted with other variables as well. Eckel and Mass (2005) noted the inclusion of different physics parameterization scheme with the same model produced less dispersion in the simulations than analysis with different models. However, in this study differences were still present as a result of including different physics options similar to the Schwartz et al. (2010) ensemble study with varying MP and PBL schemes.

Based on overall performance, it is suggested that WSM3_KF_YSU was the most satisfactory scheme combination for representing this squall line event. For temperature, this simulation produced a defined temperature gradient. This simulation also had a more satisfactory representation of the warm air advection (WAA) into central Tennessee and over Mesonet site locations (Fig. 2.6a-b).

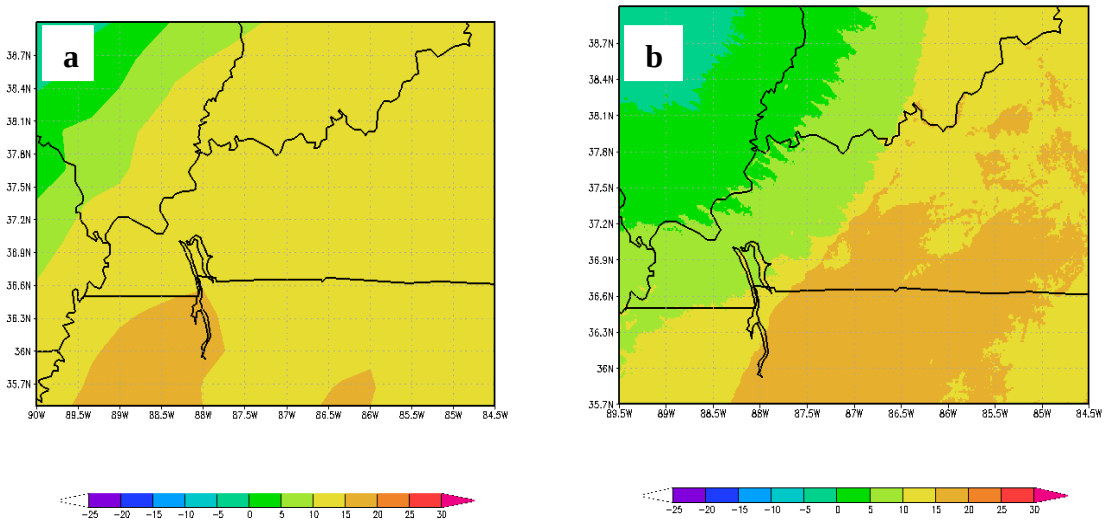

Fig. 2.6. Modeled temperature at 0000Z January 30, 2008: a) NARR b) with WSM3_KF_YSU scheme combination.

The preferred model simulation (WSM3_KF_YSU) produced the most satisfactory distribution of precipitation across the region. For example, the preferred scheme combination simulated rainfall over western sections of the domain, which several of the other model simulations did not produce. This preferred combination (WSM3_KF_YSU) showed the precipitation over the Ohio River Valley which also was not defined in several simulations. Finally, this simulation had the most satisfactory representation of precipitation totals over the eastern portion of the domain compared to other simulations, which were either displaced the rain bands or did not produce satisfactory quantity (Fig. 2.7 a-b).

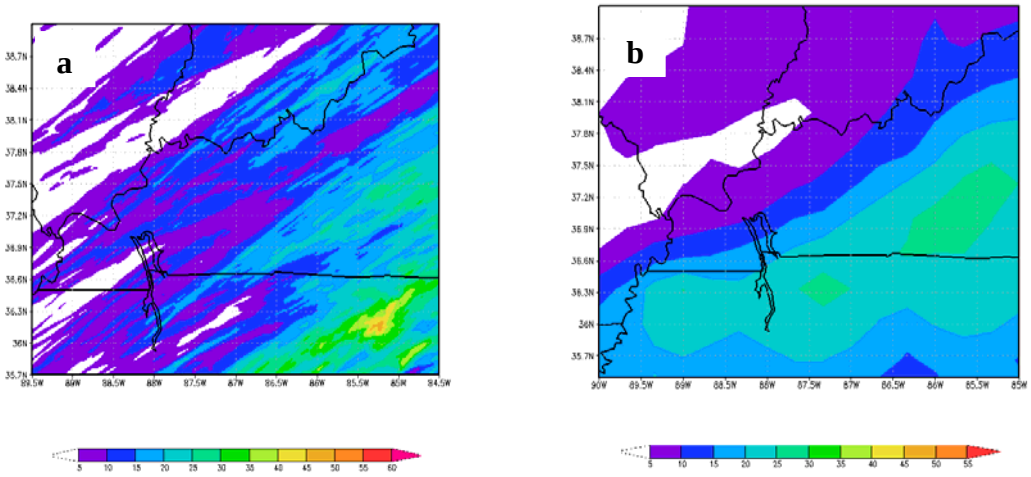

Fig. 2.7. Total precipitation from January 29, 2008 1200Z to January 30, 2008 1200Z for: a) WSM3_KF_YSU scheme combination and b) NARR.

2.5 Conclusions

The WRF model was used to produce modeled simulations of the January 29-30, 2008 Ohio Valley squall line event. Different physics parameterization scheme combinations were analyzed to determine which scheme combination produced the most satisfactory representation of this squall line event. The NARR data was used for model initialization. For each model simulation different scheme combinations of microphysics, cumulus parameterization and planetary boundary layer schemes were investigated. The data from the modeled simulations, 12 in total, were compared to the data from four Kentucky Mesonet stations. For model simulation assessment *d-index*, RMSE and r^2 were used. Simulated data were also analyzed against NARR data. As stated earlier, the WSM3_KF_YSU scheme combination was preferred.

Overall, only small differences were present in terms of different MP and CP schemes throughout all of the model simulations. However, inclusion of the YSU PBL parameter increased model accuracy in almost all cases. Future research could examine squall lines similar to this event. An example would be the January 17, 2012 squall line event which produced nine tornadoes in the lower Ohio Valley region. This severe weather event was not predicted by local meteorologists to be as extreme as it was. An investigation of other potential physics parameters with this event could provide more insight into the influence of physics scheme selections.

Chapter 3: Comparison of Initialization Data Sets Used in WRF for the January 29-30, 2008 Ohio Valley Squall Line

3.1. Model Initialization Data Sets

In Chapter Two, it was stated that through a series of simulations, certain physics parameterization schemes produced a more satisfactory representation of a squall line that passed through the lower Ohio Valley on January 29-30, 2008. This chapter provided analyses into the selection of different initialization data sets on model simulations. Overall, three different initialization data sets were examined. The North American Regional Reanalysis (NARR) (Mesinger et al. 2006), the North American Mesoscale (NAM) (Black 1994), and the Final Operational Global Analysis data set (FNL) (Kalnay et al. 1996) were used. Some of these datasets can be broken down into 1, 3 and 6-hour timesteps. Each of these datasets has unique characteristics, most notably with vertical and horizontal resolutions. The analyses with different timesteps allowed for temporal comparisons with the same dataset to see if the extra ingest and variety of data sources into WRF resulted in improved accuracy in model simulations. A brief overview of the model initialization datasets is provided below.

3.1.1. NARR

North American Regional Analysis (NARR) is a long-term, consistent, high-resolution climate dataset for North America from 1979 through present day (Mesinger et al. 2006). The NARR dataset shares some common characteristics with EDAS (Eta Data Assimilation System) which is an earlier template for the NAM dataset. However the NARR dataset has several unique characteristics that differentiate it from other datasets. NARR has a resolution of 32 km with 45 vertical layers. Another key

difference is the use of the older Eta physics package. NARR also features a fully cycled assimilation system. This system allows for the generation of a first guess for the next 3-hour block of data. Precipitation is assimilated, which allows for the conversion of latent heat. The updated technique has been shown to have a bearing on temperature and precipitation (Mesinger et al. 2006). A majority of temperature data comes from radiosondes. A drawback to use of the NARR dataset is the degree of resolution and whether it is finite enough to resolve local rainfall (Glahn 2008).

3.1.2. FNL

The FNL dataset is based on the 40-year NCEP/NCAR reanalysis project (Kalnay et al. 1996). Unlike NARR, FNL reaches back to 1957. In this dataset, horizontal resolution is around 210 km with 28 vertical levels. Data are also drawn from various sources such as radiosondes, aircraft and global telecommunication systems. Spectral statistical interpolation is used for analysis to focus on improvements in the tropics and reduce the time needed for precipitation spin-up. The T62/28 level model within the dataset includes parameterizations for all physical process, the most noteworthy is convection. Output of the data comes in four classifications. Some shortcomings regarding the FNL, suggested by Kalnay et al. (1996), include the presence of regional biases and the question of whether classifications of variables are uniformly reliable. Kalnay et al. (1996) also state that the variables are completely dependent on model output.

3.1.3 NAM

The NAM dataset is based on the Eta model, which uses a vertical coordinate system to better represent the pressure gradient force (Black 1994). Horizontal resolution with the NAM dataset is 30 km with over 50 layers in the vertical. However, the most unique aspect of NAM is that it features 1-hour intervals that can be incorporated into the WRF. Two biases were noted with the NAM dataset. The propagation speed was defined as slow compared to actual systems studied (Wang et al. 2009). Several studies noted the lack of convective precipitation or that precipitation was displaced (Etherton and Santos 2008; and Wang et al. 2009).

3.1. Literature Overview

Improvement in the model output should not be the overall expectation when increasing model resolution (Deng et al. 2004; Denis et al. 2003; Dimitrijevic and Laprise 2005; Warner et al. 1997; and Warner and Seamen 1990). The study conducted by Warner and Seamen (1990) over the northeastern United States showed that a resolution increase by a factor of three did not notably improve model performance. However, the increased resolution did allow the model to detect key mesoscale features that models with coarser resolutions may miss (Warner and Seamen 1990; and Warner et al. 1997). Another study from Deng et al. (2004) showed through use of the MM5 model that increasing horizontal and vertical resolution had a limited effect compared to use of different physics parameterization schemes. In general, changes to the horizontal and vertical resolution may improve some aspects of model simulations when using a finer resolution dataset.

Certain datasets were not used in this analysis. These include the Climate Forecast System Reanalysis (CFSR) which was not compatible with the WRF model (Suranjana et al. 2010).

3.2. Experimental Design

The WRF model is the basis for all the simulations in Chapter Three. The domains are identical to those in Chapter Two. Higher resolutions were used in this study because of the localized nature of the event in question and the desire for detailed simulations over the Mesonet locations, which are used as a comparison for the statistical analysis. The finer model resolution allowed the simulations to distinguish a majority of mesoscale features within the inner domains (Weisman et al. 1997).

Model physics parameterization schemes selected were identical throughout each simulation. Physics schemes were based on the recommendations in Chapter Two, which found that the combination of the YSU PBL, KF CP and the WSM3 MP had a satisfactory representation of this event. The data files from the NARR, FNL and NAM data source were used in WRF simulations. After completion of each WRF run, a point validation program was used (Leeper 2011 Personal communication). This program applies the WRF model output to specific geographical coordinates for selected locations. In this study the locations were the Mesonet sites in Murray, Russellville, Bowling Green and Liberty.

Model output data were then verified with surface observations. The verification process reveals if a model simulation produced a satisfactory interpretation of an atmospheric event. The comparison of modeled and surface data was numerical and

graphical. The source for surface numerical data was the Kentucky Mesonet, discussed in Chapter Two.

Model performance analyses were completed for each set of model data to compare the different simulations with the specific combination of parameterization schemes (as noted above). Statistical measures of r^2, RMSE, and an index of agreement "(*d-index*)" were used to assess model performance (Legates and McCabe 1999). The r^2 is defined as the square of the Pearson product-moment coefficient, while the RMSE is the square root of the mean square error. The analysis uses square of the Pearson method to compare modeled and Mesonet data. Values near 1.0 indicated a strong correlation while values near zero indicated no correlation. A similar scale was used for the *d-index* from zero to 1.0. Additional timeseries and graphics were generated using Excel and the Grid Analysis and Display System (GrADS). Timeseries were created to give a visual reference for comparison of model data in terms of schemes used and to compute statistical values between modeled and Mesonet values for each variable. Figures were generated in GrADS to show the distribution of precipitation with NARR as a reference. GrADS allowed the visualization of modeled meteorological variables (Institute of Global Environment and Society 2011).

3.3. Results

Overall, the differences in the selection of the initialization dataset and timestep produced a wide range of results. No selections were preferred based on the analysis of the datasets used in the WRF simulation or the timestep of any dataset. In some cases one dataset at a certain timestep was preferred for one location, and yet proved not to be the most satisfactory dataset and timestep interval for other locations or variables.

3.4.1. Comparison of FNL6-, NARR6- and NAM6-hour dataset based simulations

A comparison of the FNL6-hour, the NARR6-hour, dataset and the NAM6-hour datasets indicated small differences in model output based on the selection of initialization dataset.

Table 3.1. Comparison of model datasets with 6-hour timesteps. (Bolded statistics indicate values that are the most satisfactory for performance evaluation for each near surface atmospheric variable.)

		Temperature			Total Precipitation			Relative humidity			Dewpoint temperature		
Location	Initialization data set	*d*-index	r^2	RMSE (°C)	*d*-index	r^2	RMSE (mm)	*d*-index	r^2	RMSE (%)	*d*-index	r^2	RMSE (°C)
Bowling Green	FNL6	0.97	0.98	1.68	0.97	0.64	7.14	0.71	0.58	8.65	0.98	0.98	1.78
	NARR6	0.95	0.98	2.23	0.96	0.64	7.72	0.82	0.76	7.58	0.96	0.96	2.25
	NAM6	**0.98**	**0.99**	**1.23**	**0.98**	**0.71**	**5.28**	**0.90**	**0.86**	**6.16**	**0.99**	**0.98**	**1.00**
Murray	FNL6	0.88	0.96	4.05	0.44	0.71	7.72	0.81	0.69	8.80	0.94	0.95	3.60
	NARR6	0.80	0.93	5.18	**0.48**	**0.67**	**7.35**	0.85	0.87	9.50	0.94	0.97	3.60
	NAM6	**0.90**	**0.97**	**3.82**	0.31	0.73	9.71	0.79	0.92	12.00	**0.99**	**0.99**	**1.93**
Liberty	FNL6	0.96	0.90	2.69	0.88	0.84	10.60	0.99	0.59	9.06	0.99	0.91	1.50
	NARR6	0.99	0.88	2.77	0.89	0.78	10.22	0.99	0.61	9.03	0.99	0.90	1.53
	NAM6	**0.98**	**0.94**	**2.19**	**0.93**	**0.89**	**8.16**	**0.99**	**0.55**	**8.72**	**0.99**	**0.92**	**1.33**
Russellville	FNL6	0.97	0.98	2.47	**0.95**	**0.78**	**4.50**	0.81	0.70	8.17	0.96	0.98	2.61
	NARR6	0.94	0.97	10.45	0.93	0.84	5.99	0.86	0.85	6.87	0.95	0.98	3.13
	NAM6	**0.98**	**0.99**	**1.93**	0.93	0.79	7.00	**0.94**	**0.91**	**4.92**	**0.98**	**0.99**	**1.79**

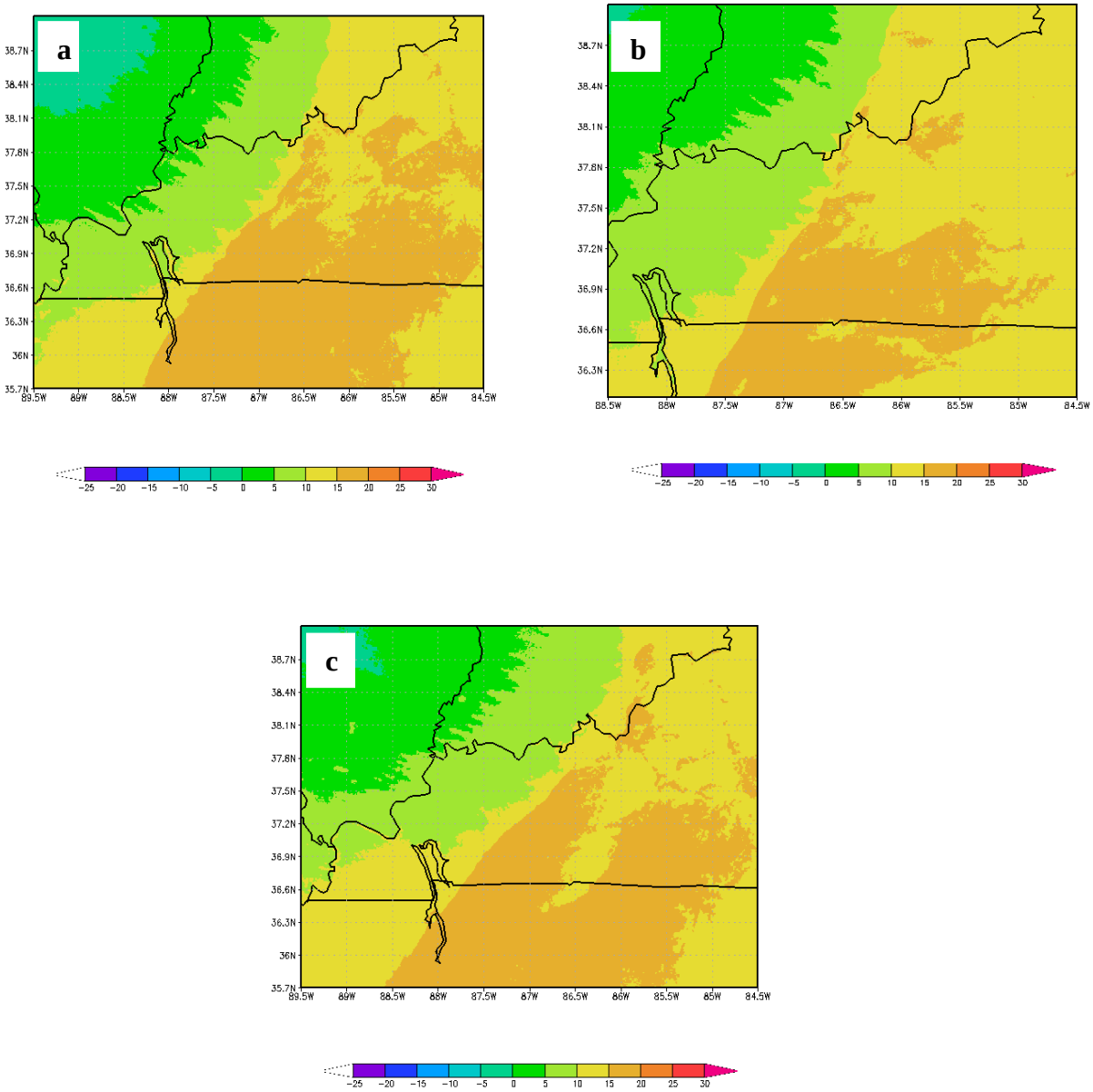

Fig. 3.1. Modeled temperature at 0000Z Janurary 30, 2008 for: a) FNL6 b) NAM6 and c) NARR6.

Total precipitation and relative humidity showed more spread in the data. For precipitation, lower *d-index* values were shown for Murray regardless of the dataset. The NAM6 produced the lowest *d-index* (Table 3.1). Initialization with the NAM6 dataset produced the highest RMSE values for Murray and Russellville but produced the lowest RMSE values at the other sites. The RMSE for precipitation totals based on FNL and NARR6 simulations were higher and lower for Liberty and Russellville respectively. Overall, the r^2 values ranged from 0.60 and 0.85 for precipitation at all locations. The simulation with the NAM6 dataset produced more satisfactory results. Seven of seven potential comparisons for temperature, four of six for relative humidity, four of four for dewpoint temperature and three of seven comparisons for precipitation resulted in higher r^2, lower RMSE and a higher *d-index* (Table 3.1). The figures below visually show there were only small differences between FNL6 and NARR6. Larger differences were present for the simulation with the NAM dataset in regards to placement of higher precipitation totals (Fig. 3.2). The WRF simulation with the NAM6 resulted in precipitation totals that were considerably higher across north central Kentucky and southern Indiana. The NAM6 simulation did not have a high bias maximum in Tennessee when compared to the other data sets.

With respect to dewpoint temperature, the use of NAM6 initialization produced statistically superior results at all four locations in terms of the RMSE. For example, RMSE values ranged from 1 °C at Bowling Green to 1.93 °C at Murray. This compared to RMSE values over 3 °C at Murray and Russellville with the FNL6 and NARR6. The r^2

and *d-index* values were above 0.90 in all cases (Table 3.1). RMSEs for FNL6 and NARR6, were 1.50 and 1.53 °C for Liberty, respectively. They were 1.78 and 2.25 °C for Bowling Green, respectively (Table 3.1).

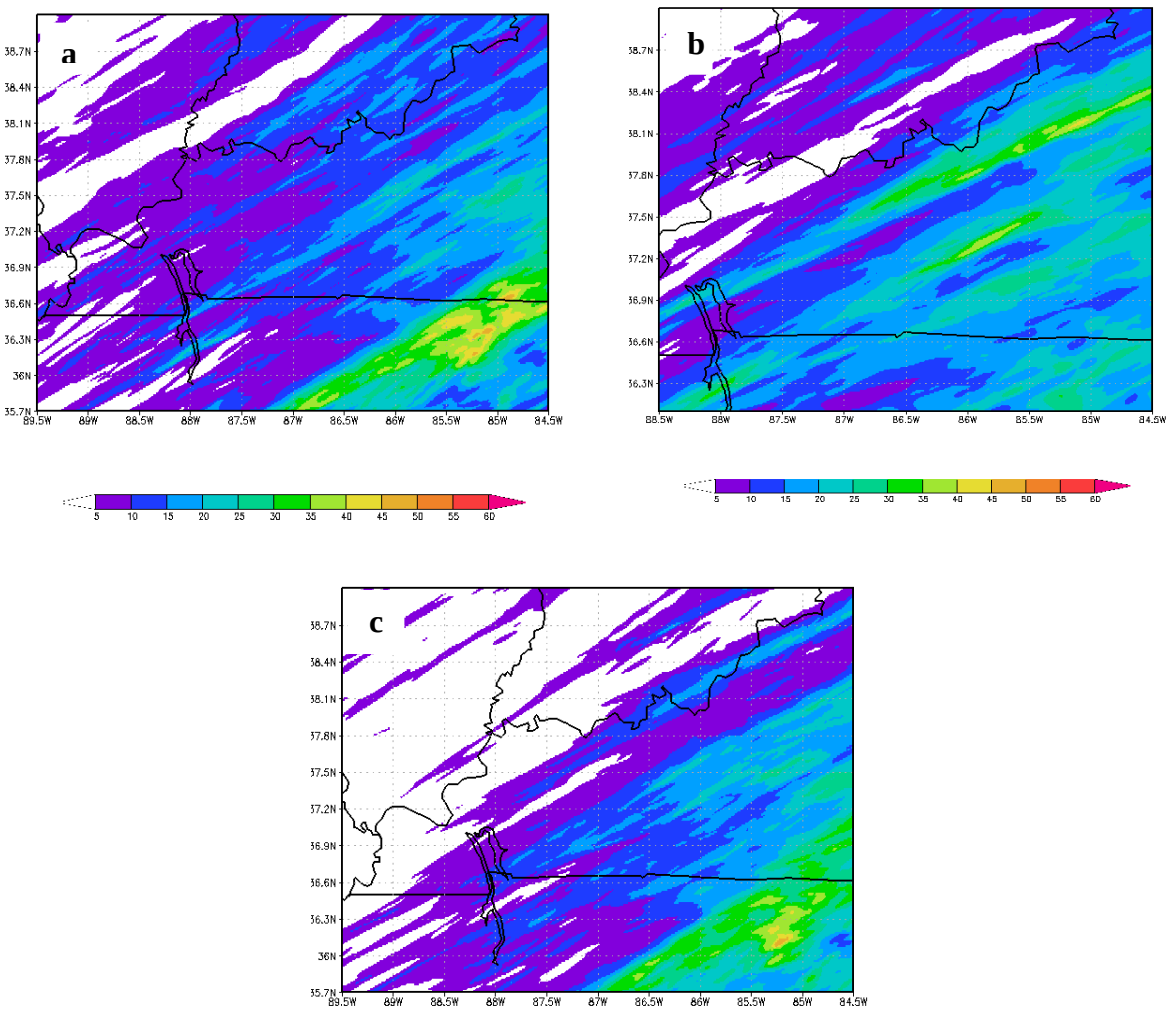

Fig. 3.2. Total modeled precipitation from 1200Z January 29, 2008 to 1200Z January 30, 2008 for: a) FNL6, b) NAM6, and c) NARR6.

3.4.2. Comparison of NARR3- and NAM3-hour dataset based simulations

A comparison of simulations with the NARR 3-hour and NAM 3-hour for temperature yielded that the *d-index* was about 0.95 for all locations for the NAM3 dataset, while the *d-index* was only about 0.70 for the NARR3 dataset at all locations (Table 3.2). The only exception was Bowling Green where RMSE values were about 2 °C lower with the NAM3 dataset. The model simulation initialization with the NAM3 dataset also had r^2 values were about 0.10 higher for temperature (Table 3.2). Visually, the NAM3 has a more defined temperatures gradient across western Kentucky at the time of squall line passage (Fig. 3.3).

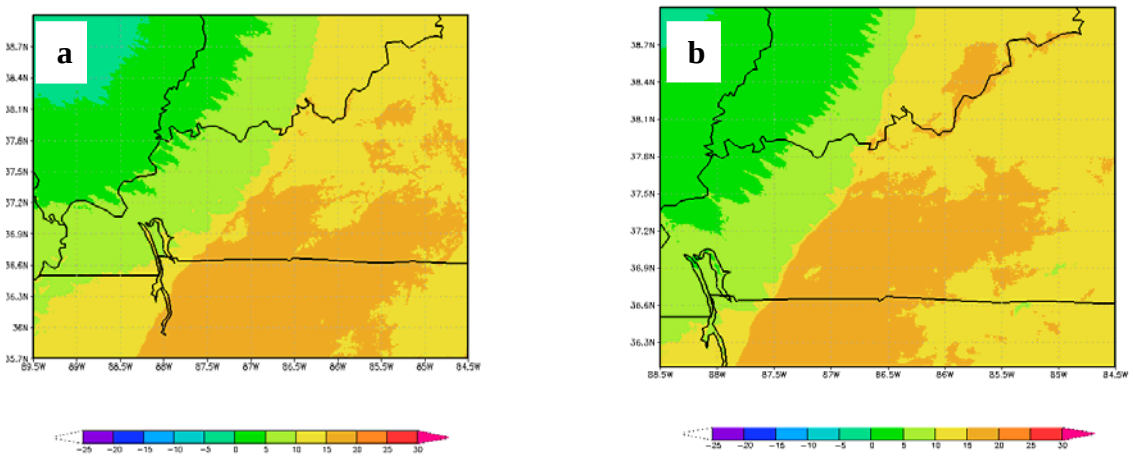

Fig. 3.3. Modeled simulation of temperature in °C at 0000Z January 30, 2008: with a) NARR3, and b) NAM3.

Table 3.2. Comparison of 3-hour datasets NARR and NAM. (Bolded statistics indicate values that are the most satisfactory for performance evaluation for each near surface atmospheric variable.)

		Temperature			Total Precipitation			Relative humidity			Dewpoint Temperature		
Location	Initialization data set	*d*-index	r^2	RMSE (°C)	*d*-index	r^2	RMSE (mm)	*d*-index	r^2	RMSE (%)	*d*-index	r^2	RMSE (°C)
Bowling Green	NARR3	0.95	0.87	4.07	0.63	**0.97**	9.11	0.71	0.54	11.16	0.78	0.92	5.50
	NAM3	**0.98**	**0.97**	**1.49**	**0.96**	0.71	**7.36**	**0.72**	**0.56**	**8.73**	**0.99**	**0.98**	**1.50**
Murray	NARR3	0.69	0.89	6.10	0.28	0.64	12.37	0.81	0.50	9.67	0.81	0.87	6.96
	NAM3	**0.91**	**0.96**	**3.58**	**0.60**	**0.75**	**5.76**	**0.85**	**0.86**	**9.33**	**0.98**	**0.97**	**2.18**
Liberty	NARR3	0.69	0.76	3.61	**0.80**	**0.96**	**8.93**	0.66	0.38	7.35	0.73	0.73	4.18
	NAM3	0.97	**0.92**	**2.33**	0.87	0.90	11.00	**0.99**	**0.64**	**8.94**	**0.99**	**0.90**	**1.48**
Russellville	NARR3	0.76	0.86	4.93	0.58	0.94	6.26	0.74	0.67	10.52	0.80	0.90	6.36
	NAM3	**0.98**	**0.97**	**2.00**	**0.99**	**0.89**	**2.19**	**0.87**	**0.85**	**6.17**	**0.98**	**0.98**	**2.15**

For precipitation, the *d-index* values for Murray for the NARR3 had a very low index of agreement of 0.28, coupled with a high RMSE of 12.37 mm. However, at all the other locations a satisfactory correlation above 0.90 was noted with WRF simulations that used the NARR3 dataset (Table 3.2).

For relative humidity, the WRF simulation with the NAM3 dataset produced lower RMSE and higher r^2 values at all locations (Table 3.2). Similar results occurred with respect to dewpoint temperature. Overall, *d-index* and r^2 values were close to 1.0 with the NAM3 dataset simulation while they only ranged between 0.80-0.90 with the simulation using the NARR3 dataset (Table 3.2). For dewpoint temperature, simulations with the NAM3 resulted in *d-index* and r^2 close to one for most locations.

Overall, the NAM3 dataset produced higher r^2 and *d-index* values along with a lower RMSE for most comparisons between the two datasets. In summary, 12 of 12 comparisons for temperature and dewpoint temperature, 11 of 12 comparisons for relative humidity and 9 of 12 comparisons for precipitation showed that the NAM3 was a more satisfactory dataset.

3.4.3. Comparison of NARR3- and NARR6-hour dataset based simulations

For temperature, the WRF simulations with the NARR3 data had a lower *d-index* and r^2 values than the NARR6. However, the RMSEs include both low and high values and ranged from 2.23 to 10.45 for the model simulations with the NARR6 data set.

Table 3.3. Comparison of model simulation with NARR datasets at different timesteps. (Bolded statistics indicate values that are the most satisfactory for performance evaluation for each near surface atmospheric variable.)

Location	Initialization data set	Temperature			Total Precipitation			Relative humidity			Dewpoint temperature		
		d-index	r^2	RMSE (°C)	*d-index*	r^2	RMSE (mm)	*d-index*	r^2	RMSE (%)	*d*-index	r^2	RMSE (°C)
Bowling Green	NARR3	0.95	0.87	4.07	0.63	0.97	9.11	0.71	0.54	11.16	0.78	0.92	5.50
	NARR6	**0.95**	**0.98**	**2.23**	**0.96**	**0.64**	**7.72**	**0.82**	**0.76**	**7.58**	**0.96**	**0.96**	**2.25**
Murray	NARR3	0.69	0.89	6.10	0.28	0.64	12.37	0.81	0.50	9.67	0.81	0.87	6.96
	NARR6	**0.80**	**0.93**	**5.18**	**0.48**	**0.67**	**7.35**	**0.85**	**0.87**	**9.50**	**0.94**	**0.97**	**3.60**
Liberty	NARR3	0.69	0.76	3.61	0.80	0.96	8.93	**0.66**	**0.38**	**7.35**	0.73	0.73	4.18
	NARR6	**0.99**	**0.88**	**2.77**	0.89	0.78	10.22	0.99	0.61	9.03	**0.99**	**0.90**	**1.53**
Russellville	NARR3	**0.76**	**0.86**	**4.93**	0.58	0.94	6.26	0.74	0.67	10.52	0.80	0.90	6.36
	NARR6	0.94	0.97	10.45	**0.93**	**0.84**	**5.99**	**0.86**	**0.85**	**6.87**	**0.95**	**0.98**	**3.13**

Graphical representations of temperature show small differences between the NARR3 and NARR6 datasets in general (Fig. 3.4.).

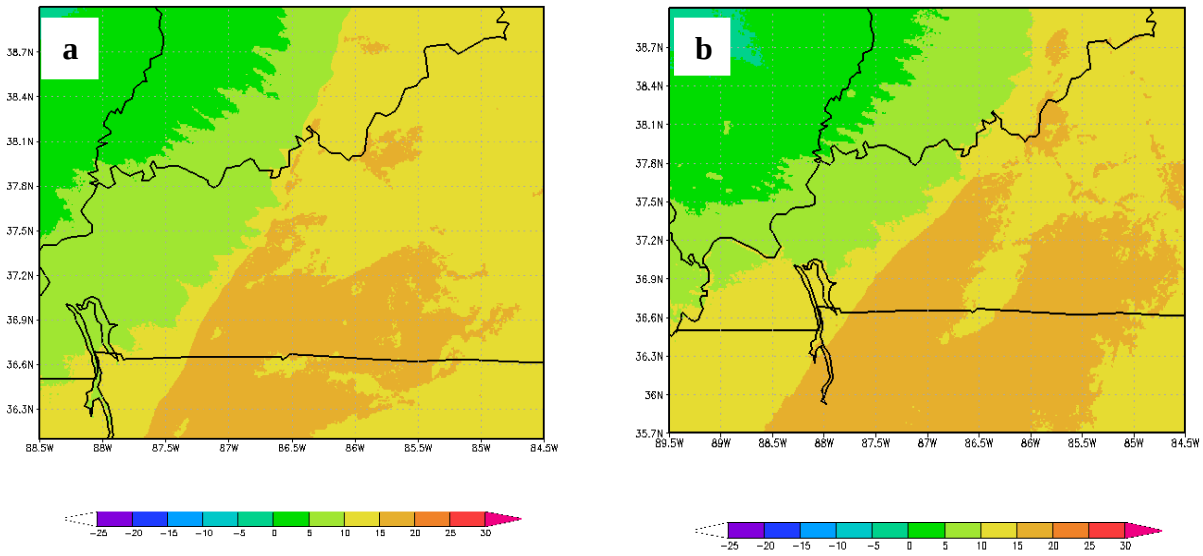

Fig. 3.4. Temperature at 0000Z Janurary 30, 2008 in °C for: a) NARR3, b) NARR6.

For precipitation, RMSE values were over 0.90 at Bowling Green and Russellville for simulations with the NARR6 dataset. While with the NARR3 dataset r^2 values were above 0.90 at all locations except for Murray (Table 3.3 and Fig. 3.5).

For relative humidity, there was slightly more consistency in the NARR6 showing more desired statistical values. The *d-index* was higher at all locations for relative humidity, mostly around 0.80, against the values around 0.70 from the NARR3 simulation (Table 3.3). This pattern of agreement could be extended to the r^2 values. For example, at Liberty shows an r^2 with the NARR3 dataset-based simulations of only 0.38, while a value of 0.61 was found for the NARR6 dataset.

In regards to dewpoint temperature, the model simulations with the NARR6 initialization dataset and their comparisons with the observed data resulted in lower RMSE values, a higher *d-index* and higher r^2 values at all locations. The *d-index* were about 0.95 for the NARR6 dataset while only about 0.70 to 0.80 for the NARR3 (Table 3.3). RMSE's for the NARR6 dataset were about half of the NARR3 dataset. For example, at Bowling Green, the RMSE was 5.5 °C with the NARR3 and 2.25 °C with the NARR6 dataset, respectively (Table 3.3).The *d-index* values were just close to 1.0 with the NARR6 and NARR3 datasets. The r^2 values were fairly similar for simulations with the NARR6 resulting in only slightly higher values compared to simulations using the NARR3 dataset, with the exception for Liberty.

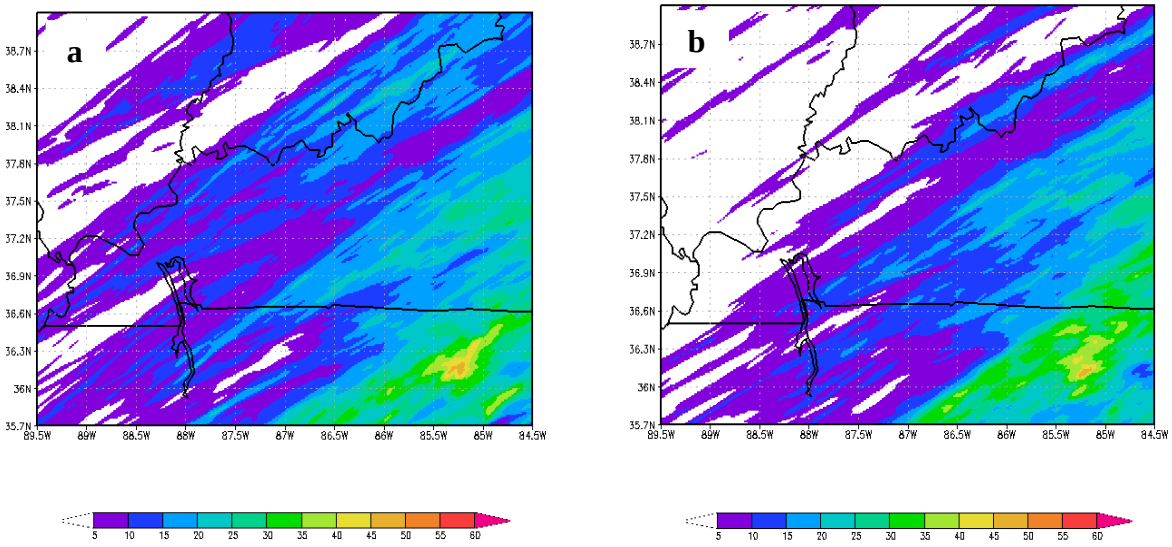

Fig.3.5. Modeled simulation for total precipitation with: a) NARR3 and b) NARR6.

In summary, between NARR3 the NARR6, it is suggested that the latter would be a preferable initialization dataset for this squall line case. Overall, 12 of 12 statistical comparisons for modeled and observed temperature, 10 of 12 for relative humidity and 11 of 12 comparisons for dewpoint temperature showed that that use of NARR6 produced relatively more satisfactory results.

3.4.4. Comparison of NAM1-, NAM3-, and NAM6-hour dataset based simulations

For temperatures, all locations showed small differences in the simulations performance evaluation statistics regardless of which NAM dataset was used. The *d-index* and r^2 values were quite high and were around 0.90. There were also small differences with RMSE values as well. For example, RMSE values for Bowling Green only ranged from 1.23 °C to 1.56 °C (Table. 3.4.). Visually, the temperature gradient

appears to be more satisfactorily resolved as the timestep length decreases. However, there was only a small difference between the temperatures at the time of squall line passage on each of the NAM simulations (Fig. 3.6).

Table 3.4. Comparison of NAM datasets. (Bolded statistics indicate values that are the most satisfactory for performance evaluation for each near surface atmospheric variable.)

		Temperature			Total Precipitation			Relative Humidity			Dewpoint Temperature		
Location	Initialization data set	*d-index*	r^2	RMSE (°C)	*d-index*	r^2	RMSE (mm)	*d-index*	r^2	RMSE (%)	*d-index*	r^2	RMSE (°C)
Bowling Green	NAM1	**0.98**	0.97	1.56	0.95	0.67	**1.56**	0.60	0.48	9.43	**0.99**	**0.98**	1.42
	NAM3	**0.98**	0.97	1.49	0.96	0.71	7.36	0.72	0.56	8.73	**0.99**	**0.98**	1.50
	NAM6	**0.98**	**0.99**	**1.23**	**0.98**	**0.71**	5.28	**0.90**	**0.86**	**6.16**	**0.99**	**0.98**	**1.00**
Murray	NAM1	0.85	0.83	4.40	0.56	0.69	6.53	0.67	0.40	10.13	0.84	0.76	5.57
	NAM3	**0.91**	**0.96**	**3.58**	**0.60**	**0.75**	**5.76**	**0.85**	0.86	**9.33**	0.98	0.97	2.18
	NAM6	0.90	0.97	3.82	0.31	0.73	9.71	0.79	**0.92**	12.00	**0.99**	**0.99**	**1.93**
Liberty	NAM1	0.97	**0.92**	**2.29**	0.87	0.86	11.22	**0.99**	0.52	**8.65**	**0.99**	0.89	1.54
	NAM3	0.97	0.92	2.33	0.87	0.90	11.00	**0.99**	**0.64**	8.94	**0.99**	0.90	1.48
	NAM6	**0.98**	0.94	2.19	**0.93**	**0.89**	**8.16**	**0.99**	0.55	8.72	**0.99**	**0.92**	**1.33**
Russellville	NAM1	0.98	0.96	2.08	0.97	0.77	3.77	0.77	0.66	8.20	**0.98**	0.97	1.99
	NAM3	0.98	0.97	2.00	0.99	0.89	2.19	0.87	0.85	6.17	**0.98**	0.98	2.15
	NAM6	**0.98**	**0.99**	**1.93**	0.93	0.79	7.00	**0.94**	**0.91**	**4.92**	**0.98**	**0.99**	**1.79**

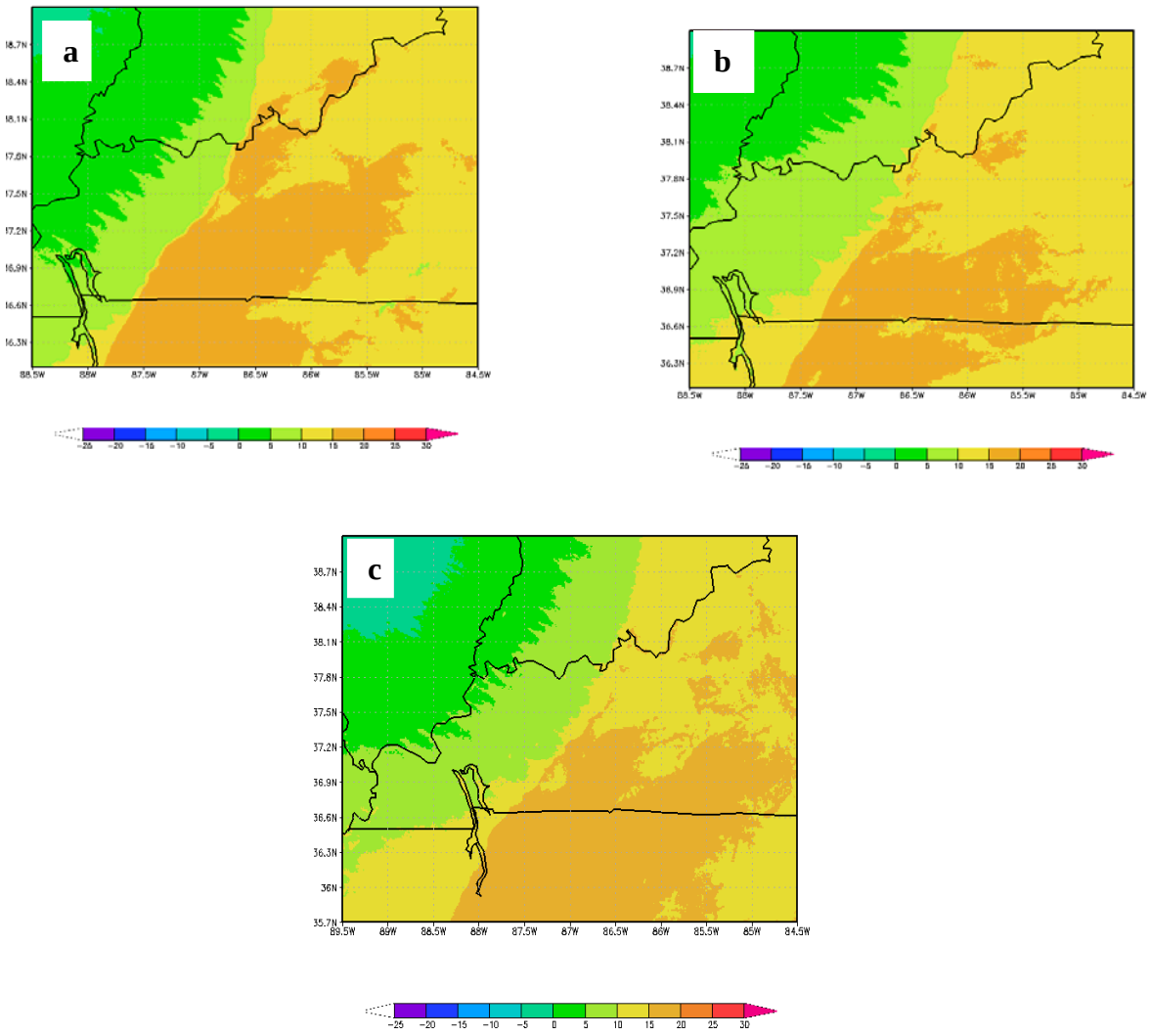

Fig. 3.6. Modeled temperature at 0000Z January 30, 2008 for a) NAM1 b) NAM3 and, c) NAM6.

For precipitation and relative humidity, there was no clearly superior dataset. The NAM6 produced the smallest (6.16%) RMSE for relative humidity for Bowling Green and the largest for Murray (12%) (Table 3.4). Use of NAM6 produced higher r^2 for all

locations except for Liberty, while the use of the NAM1 resulted in the lowest r^2 values. For example, an r^2 of 0.99 was found for Bowling Green for temperature and a r^2 of 0.69 was found for Murray for precipitation (Table 3.4). The use of NAM3 produced higher *d-index* values for Murray, 0.85 for precipitation while the use of NAM6 provided higher *d-index* values for Bowling Green and Russellville.

With the use of different NAM data sets, it was found that the RMSEs for Bowling Green were only 0.50 °C apart in Bowling Green for dewpoint temperature. The r^2 and *d-index* values were close to 1.0 at all locations besides Murray (Table 3.4). For precipitation, initialization of the model with the NAM1 dataset produced a low RMSE of 1.42 mm and a high r^2 value of 0.98 at Bowling Green. The NAM6 had the highest *d-index* for Liberty and Murray, respectively. In short, there were no clear-cut superior outcomes for precipitation when these data sets were used. Overall, these model simulations appeared to produce clearer banded mesoscale features than model simulations using all the other datasets (Fig. 3.7).

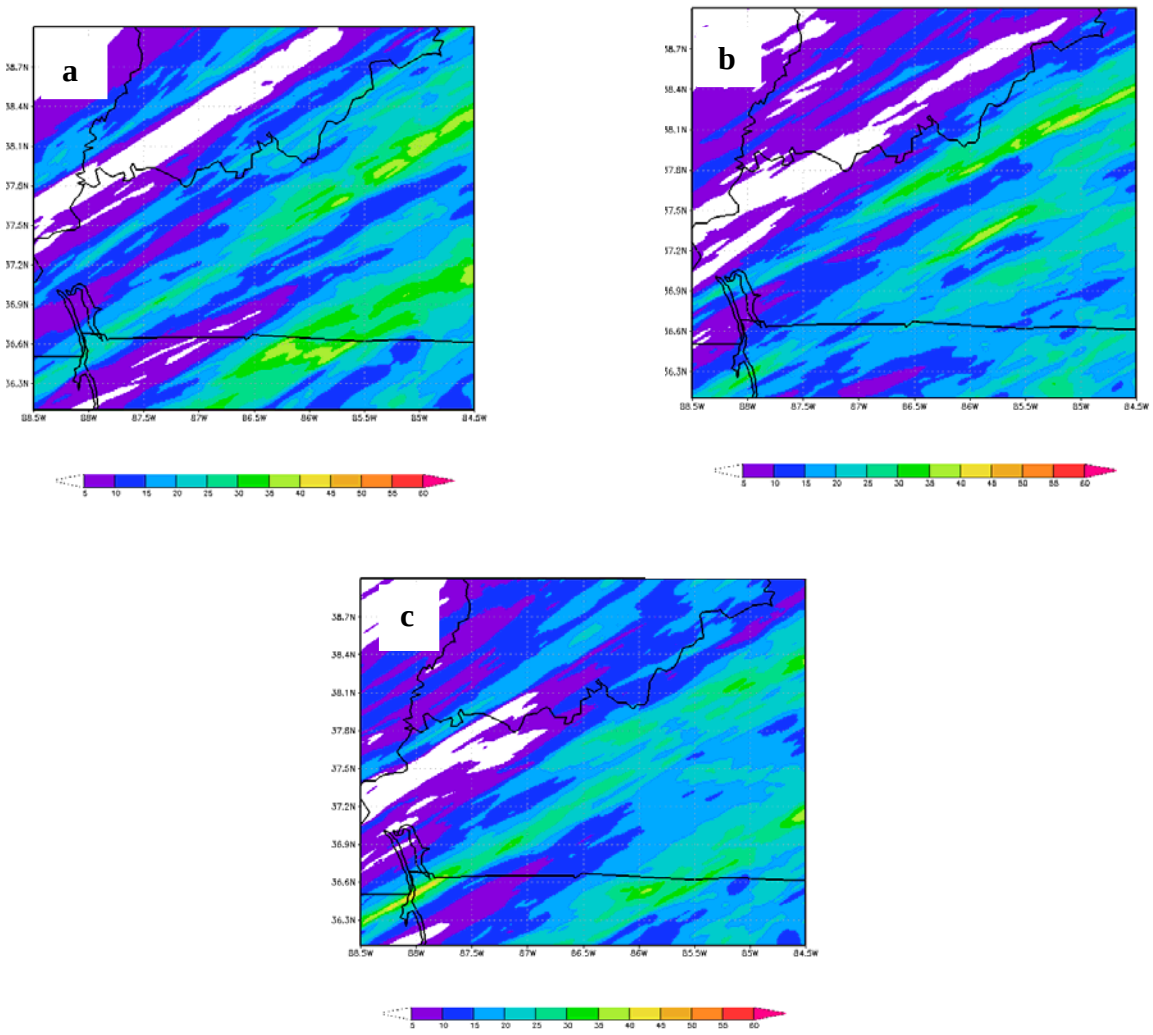

Fig. 3.7. Modeled total Precipitation with the: a) NAM1, b) NAM3, and c) NAM6.

In general, the differences among model simulations using the NAM1, NAM3, and NAM6 datasets were small. The NAM6, however, produced more satisfactory data in 10 out of 19 potential cases.

3.5. Conclusion

Overall, no clear superior dataset was found for the WRF simulations with a particular dataset for this squall line event. One dataset may be better in handling temperatures at one location, but another dataset may be preferred at other locations. These findings concur with the literature that an increase in timesteps in initialization datasets may not result in improvement in model simulations (Deng et al. 2004; Denis et al. 2003; Dimitrijevic and Laprise 2005; Warner et al. 1997; and Warner and Seamen 1990). In some cases a slight preference toward the NAM datasets were observed. This observation of somewhat slightly superior results is likely linked to the increased vertical layers and horizontal resolution. This corresponds to previous research which shows improved resolution can have an influence on model results (Deng et al. 2004; Denis et al. 2003; Dimitrijevic and Laprise 2005; Warner et al. 1997; and Warner and Seamen 1990). The increased resolution did allow the model to detect key mesoscale features that models with coarser resolutions may miss (Warner and Seamen 1990; and Warner et al. 1997). This is noted in the NAM graphics that detected banded precipitation and higher temperature gradients with modeled simulations (Fig. 3.7). An increase in the gradients was even more defined with the shorter timesteps. It should be noted that even with more defined temperature gradients and precipitation maps, the overall model performance did not show the shorter timesteps to be more accurate.

Chapter 4: Summary

This research used the WRF to simulate the atmosphere for January 29-30, 2008, when a squall line moved over the Ohio Valley region. Different physics parameterization scheme combinations were used in the WRF for a total of 12 simulations. It was found that the simulations with the WSM3 microphysics, KF cumulus parameterization, and YSU PBL scheme combination were preferred. The YSU PBL features the inclusion of an explicit treatment of entrainment process layer at the top of the PBL. This entrainment process leaves more fuel for the accurate representation of severe convection (Hong et al. 2006). The MYJ PBL on the other hand, has a local diffusion scheme which has a strong tendency to underdevelop convection due to a strong capping inversion (Ayotee et al. 1996). The KF scheme has been documented to have a better interpretation with regards to convective case studies, while the BMJ CP scheme sometimes exaggerates light areas of precipitation (Jankov et al. 2005). With regards to MP, the difference in class structure had little effect in this case study with the WSM having a more favorable visual comparison with fewer class groupings.

After selection of WSM3_KF_YSU combination, different model initialization datasets were used to determine which dataset produced the most satisfactory simulation. For this purpose, six additional simulations were conducted to show the effect of using different sets of initialization data and timesteps. Overall, it was found that differences in the initialization dataset did not have a noticeable influence on model simulations. These findings were similar to Tapiador et al. (2012) and Deng et al. (2004). However, the higher resolutions of the NAM datasets allowed the model simulations to have more defined mesoscale features in some cases (e.g., temperature).

Events such as this squall line (January 29-30, 2008) are unusual. However, on January 17, 2012, another squall line with similar synoptic and mesoscale meteorological conditions occurred across the region. The majority of weather forecasters and the general public were unaware of the severe threat until just a few hours before it occurred. Nine tornadoes affected southern Indiana and Kentucky. Improved WRF simulations of these types of events will lead to forecaster excellence and heightened public awareness.

REFERENCES

Ayotee, K., P. Sullivan, A. Andren, S. Doney, A. Holtslag, W. Large, J. McWilliams, C. Moeng, M. Otee, J. Tribbia, and J. Wyngaard, 1996: An evaluation of neutral and convective planetary boundary layer parameterizations relative to large eddy simulations. *Boundary layer Meteorology*, **79**, 131-175.

Betts, A., 1986: A new convective adjustment scheme. Part 1: observational and theoretical basis. *Quarterly Journal of the Royal Meteorological Society*, **112**, 677-691.

Betts, A., M. Miller, 1986: A new convective adjustment scheme. Part 2: single column tests using the GATE wave, BOMEX, ATEX, and arctic air-mass data sets., *Quarterly Journal of the Royal Meteorological Society*, **112**, 693-709.

Black, T., 1994: The new NMC mesoscale ETA model: description and forecast examples. *Weather Research and Forecasting*, **9,** 265–278.

Brown, Z., S. Foster, R. Mahmood, S. Struebig, D. Grabowski, M. Grogan, and M. Ferris, An overview of the Kentucky Mesonet. *17th Conference on Applied Climatology*, Whistler, BC, American Meteorological Society.

Denis, B., R. Laprise, and D. Caya, 2003: Sensitivity of a regional climate model to the resolution of lateral boundary conditions. *Climate Dynamics*, **20**, 107-126.

Deng, A., N. Seaman, G. Hunter, and D. Stauffer, 2004: Evaluation of interregional transport using the MM5-SCIPUFF system. *Journal of Applied Meteorology*, **43**, 1864-1886.

Dimitrijevic, M., and R. Laprise, 2005: Validation of the nesting technique in a regional climate model and sensitivity tests to the resolution of the lateral boundary conditions during summer. *Climate Dynamics*, **25**, 555-580.

Dudhia, J., 1989: Numerical study of convection observed during the winter monsoon experiment using a mesoscale two-dimensional model. *Journal of Atmospheric Science*, **46**, 3077–3107.

Eckel, A., and C. Mass, 2005: Aspects of effective mesoscale, short-range ensemble forecasting. *Weather Research and Forecasting*, **20**, 328–350.

Etherton, B., P. Santos, 2008: Sensitivity of WRF forecasts for South Florida to initial conditions. *Weather Research and Forecasting*, **23**, 725–740.

Gallus, W. A., 1999: Eta simulations of three extreme precipitation events: sensitivity to resolution and convective parameterization. *Weather Research and Forecasting*, **14**, 405–426.

Gallus, W. A., and J. F. Bresch, 2006: Comparison of impacts of WRF dynamic core, physics package, and initial conditions on warm season rainfall forecasts. *Monthly Weather Review*, **134**, 2632-2641.

Glahn, B., 2008: Reforecasts: An important dataset for improving weather predictions. *Bulletin of the American Meteorological Society*, **89**, 1373–1376.

Grell, G., and D. Devenyi, 2002: A generalized approach to parameterizing convection combining ensemble and data assimilation techniques. *Geophysical Research Letters*, **29,** 14.

Houze, R., M. Biggerstaff, S. Rutledge, B. Smull, 1989: Interpretation of Doppler Weather Radar Displays of Midlatitude Mesoscale Convective Systems. *Bulletin of the American Meteorological Society*, **70**, 608–619.

Hong, S., and H. Pan, 1996: Nonlocal boundary layer vertical diffusion in a medium range forecast model. *Monthly Weather Review*, **124**, 2332-2339.

Hong, S., J. Dudhia and S. Chen, 2004: A revised approach to ice microphysical processes for the bulk parameterization of clouds and precipitation. *Monthly Weather Review*, **132**, 103–120.

Hong, S., Y. Noh, and J. Dudhia, 2006: A new version with an explicit treatment of entrainment process. *Monthly Weather Review*, **134**, 2318-2341.

Hong, S., and J. Lim, 2006: The WRF 6-class microphysics scheme (WSM6). *Journal of the Korean Meteorological Society*, **42**, 129-151.

Hong, S., and S. Kim, 2007: Stable boundary layer mixing in a vertical diffusion scheme Seoul, Korea, The Korea Meteorological Society Fall Conference.

Hydrometeorological Prediction Center 2010: [Available online at www.hpc.ncep.noaa.gov].

Hu, M., J. Gammon, and F. Zhang, 2010: Evaluation of three planetary boundary layer schemes in the WRF Model. *Journal of Applied Meteorology and Climatology*, **49**, 1831–1844.

Insitute of Global Environmental Society Cited 2011: Grads [Available online at http://www.iges.org/grads/grads.html].

Janjić, I., 1990: The step-mountain coordinate: physical package. *Monthly Weather Review*, **118**, 1429–1443.

Jankov, I., W. Gallus., M. Segal, B. Shaw, and S.Koch, 2005: The impact of different WRF model physical parameterizations and their interactions on warm season MCS rainfall. *Weather Research and Forecasting*, **20**, 1048-1060.

Kain, J., and J. Fritsch, 1990: A one dimensional entraining/detraining plume model and its application in convective parameterization , *Journal of the Atmospheric Sciences*, **47**, 2784-2802.

Kain, J., 2004: The Kain-Fritsch convective parameterization: an update, *Journal of Applied meteorology*, **43**, 170-181.

Kalnay, E., M. Kanamitsu, R. Kistler, W. Collins, D. Deaven, L. Gandin, M. Iredell, S.Saha, G. White, J. Woollen, Y. Zhu, M. Chelliah, W. Ebisuzaki, W. Higgins, J. Janawiak, K. Mo, C. Ropelewski, J. Wang, A. Leetmaa, R. Reynolds, R. Jenne and D. Joesph, 1996: The NCEP/NCAR 40-Year Reanalysis Project, *Bulletin of the American Meteorological Society,* **77**, 437-471.

Kessler, M., A. Anderson and G. Stock, 2006: Modeling topographic and climatic control of east-west asymmetry in Sierra Nevada glacier length during the last glacial maximum. *Journal of Geophysical Research-Earth Surface,* **111,** (F2).

Legates, D., and G. McCabe, 1999: Evaluating the use of "goodness-of-fit" measures in hydrologic and hydroclimatic model validation, *Water Resources Research*, **35**, 233-241.

Lin,Y., R. Farley, and H. Orville, 1983: Bulk parameterization of the snow field in a cloud model, *Journal of Climate and Applied Meteorology*, **22**, 1065-1092.

Mahmood, R., B. Jordan, D. Klunk, D. Mock, P. Schulz, G. Takle, and S. Wash, 2008: The Kentucky Mesonet: Background and future applications. In the Corn and Climate Report: A practical guide to help midwestern farmers understand and respond to a changing climate. S. Ames, IA: Iowa State University, 18-19.

Mccumber, M., Tao, W. K., J. Simpson, R. Penc, and S. Soong, 1991: Comparison of ice microphysical parameterization schemes using numerical simulations of tropical convection. *Journal of Applied meteorology*, **30**, 985-1004.

Meted Cited: 2012 [Available online at http://www.meted.ucar.edu/convectn/mcs/index.htm].

Mesinger, F., G. Dimego, E. Kalnay, K. Mitchell, P. Shafran, W. Ebisuzaki, D. Jovic, J. Woollen, E. Rodgers, E. Berbery, E. Fan, R. Grumbine, W. Higgins, H. Li, Y. Lin, G. Manikin, D. Parrish, and W. Shi, 2006: North American Regional Reanalysis. *Bulletin of the American Meteorological Society*, **87**, 343–360.

National Climatic Data Center Cited: 2012 Storm Data [Available online at http://www.ncdc.noaa.gov/oa/climate/sd/].

National Weather Service Louisville, KY Cited: 2012 jet streak diagram [Available online at http://www.crh.noaa.gov/lmk/soo/docu/forcein.gif].

National Weather Service Weather glossary Cited: 2012, [Available online at http://forecast.weather.gov/glossary.php?].

Newton, C., 1950: Structure and mechanism of the prefrontal squall line. *Journal of Meteorology*, **7**, 210-223.

Pielke, R., W. Cotton, R.Walko, C. Tremback, W. Lyons, L. Grasso, M. Nicholls, M. Moran, D. Wesley, T. Lee, and J. Copeland 1992: A comprehensive meteorological modeling system. *Meteorology and Atmospheric Physics*, **49**, 69-91.

Rajeevan, M., A. Kesarkar, S. Thampi, T. Rao, B. Radhakrishna and M. Rajasekhar., 2010: Sensitivity of WRF cloud microphysics to simulations of a severe thunderstorm event over Southeast India. *Annual Geophysics*, **28**, 603-619.

Rao, Y.V., H. Hatwar, A. K. Salah and Y. Sudhakar, 2007: An experiment using high resolution ETA and WRF models to forecast heavy precipitation events over India. *Pure and Applied Geophysics*, **164**, 1593-1615.

Rhome, J., D. Niyogi, S. Ramun. 2000: Mesoclimatic analysis of severe weather and ENSO interactions in North Carolina. *Geophysical Research* Letters, **27**, 2269-2272

Rutledge, S., and P. Hobbs, 1984: The mesoscale and microscale structure and organization of clouds and precipitation in midlatitude cyclones: A diagnostic modeling study of precipitation development in narrow cold-frontal rainbands, *Journal of the Atmospheric Sciences,* **41**, 2949-2972.

Ruiz, J., S. Celeste, and J. Nogués-Paegle, 2010: WRF model sensitivity to choice of parameterization over South America: validation against surface variables. *Monthly Weather Review*, **138**, 3342–3355.

Saha, Suranjana, and Coauthors, 2010: The NCEP climate forecast system reanalysis. *Bulletin of the American Meteorology Society*, **91***,* 1015-1057.

Sanjay, J. P., Mukhopadhyay, and S. Singh, 2002: Impact of nonlocal boundary layer diffusion scheme on forecasts over Indian region. *Meteorological Atmospheric Physics*, **80**, 207–216.

Schwartz, C., J. Kain, S. Weiss, M. Xue, D. Bright, F. Kong, K. Thomas, J. Levitt, M.Coniglio, and M.Wandishin, 2010: Toward improved convection-allowing ensembles: model physics sensitivities and optimizing probabilistic guidance with small ensemble membership. *Weather Research and Forecasting*, **25**, 263–280.

Shin, Sun-Hee, and K.Ha, 2007: Effects of spatial and temporal variations in PBL depth on a GCM. *Journal of Climate*, **20**, 4717–4732.

Skamarock, W., J. Klemp, J. Dudhia, D. Gill, X. Huang, M. Duda, D. Barker, W. Wang., and J. Powers, cited 2009: A description of the advanced WRF version 3. [Available online at http://www.wrf-model.org/wrfadmin/docs/arw_v3.pdf].

Stensrud, D., 2007: *Paramterization Schemes: Keys to Understanding Numerical Weather Prediction Models*. Cambridge University Press, 459 pp.

Storm Prediction Center Cited: 2010 [Available online at www.spc.noaa.gov/exper/archive/080129/index.html].

Tao, W.K., J. Simpson, D. Baker, S. Braun, M. Chou, B. Ferrier, D. Johnson, A. Khain, S. Lang, B. Lynn, C. Shie, D. Starr, C. Sui, Y. Wang, and P. Wetzel, 2003: Microphysics, radiation and surface processes in the Goodard Cumulus Ensemble (GCE) model. *Meteorology and Atmospheric Physics,* **82**, 97-137.

Tapiador, F., W. Tao, J. Shi, C. Angelis, M. Martinez, C. Marcos, A. Rodriguez, and A. Hou, 2012: A comparison of perturbed initial conditions and Multiphysics Ensembles in a Severe Weather Episode in Spain. *Journal of applied meteorology and climatology*, in press.

Thompson, G., R. Rasmussen, K. Manning, 2004: Explicit forecasts of winter precipitation using an improved bulk microphysics scheme. Part I: description and sensitivity analysis. *Monthly Weather Review*, **132**, 519–542.

Wang,Y., T. Chen, E. Taylor., 2009: Evaluations of NAM forecasts on midtropospheric perturbation-induced convective storms over the U.S. Northern Plains. *Weather Research and Forecasting*, **24**, 1309–1333Z

Warner, T., A. Peterson, and R. Treadon., 1997: A tutorial on lateral boundary conditions as a basic and potentially serious limitation to regional numerical weather prediction. *Bulletin of American meteorological Societ*y, **78**, 2599-2617.

Warner, T., and N. Seaman, 1990: A Real-Time, mesoscale numerical weather-prediction system used for research, teaching, and public service at The Pennsylvania State University. *Bulletin of American meteorological Society*, **71**, 792–805.

Weisman, L., W. Skamarock, and J. Klemp, 1997: The resolution dependence of explicitly modeled convective systems. *Monthly Weather Review*, **125**, 527–548.

Weisman, L., C. Davis, W. Wang, K. Manning, and J. Klemp, 2008: Experiences with 0–36-h explicit convective forecasts with the WRF-ARW model. *Weather Research and Forecasting*, **23**, 407–437.

Wilson, J., J. Wix, Z. Brown, M. Ferris, S. Foster, cited 2009: January 29, 2008 squall line. [Available online at http://www.kyMesonet.org/research.html].